Mechanics of Advanced Composite Structures

Journal homepage: https://macs.semnan.ac.ir/

Semnan University

ISSN: 2423-7043

Research Article

Forced Vibration Response of a Sandwich Cantilever Nine-Layer Microbeam with Homogeneous Core Reinforced by Nanocomposite and Piezo-Magneto-Electric Layers as a Self-Sensing Mass Sensor

Behnam Mokhtarian Dehkordi, Mehdi Mohammadimehr*

Department of Solid Mechanics, Faculty of Mechanical Engineering, University of Kashan, Kashan, Iran

**Corresponding author: Mehdi Mohammadimehr, Professor, Fax:+98 31 5591 2424, Tel:+98 31 5591 3432, Postal Code: 87317-53153, E-mail: mmohammadimehr@kashanu.ac.ir*

ARTICLE INFO

Article history:

Received: 2023-10-19
Revised: 2024-03-22
Accepted: 2024-05-12

Keywords:

Forced vibration;
Sandwich cantilever microbeam;
Self-sensing mass sensor;
Electric and magnetic fields;
Nine-layer microbeam;

ABSTRACT

The novelty of this research is to consider simultaneously forced vibration response of a nine-layer sandwich microbeam with homogeneous core reinforced by nanocomposite and piezo-magneto-electric layers under electric and magnetic fields in x and z directions as a self-sensing mass sensor at the end core layer. Also, in the present study, the natural frequencies based on two methods, including the separation of variables for different B.C.'s and Navier's method for the S-S case, are obtained. In this study, the effects of various parameters such as an added mass at the end of core, different Young's modulus to the density ratio, different properties of core, volume fraction of CNT, thickness ratio, aspect ratio, length of each layer to length of the core ratio, various distribution of carbon nanotube (CNT), material length scale parameter, electric and magnetic fields, input voltage on the frequency response function (FRF) amplitude are investigated. It shows that the natural frequency for C-C is higher than the other cases (C-S, S-S, C-F), because the stiffness of the structures increases. Moreover, it shows that the natural frequency based on modified couple stress theory (MCST) is higher than classical theory (CT), because the material length scale parameter enhances the stiffness of a sandwich beam. It illustrates that the natural frequency for the FG-X distribution is higher than for other distributions, because the stiffness of the structure at the furthest distance from the neutral axis. It shows that with an enhance in the length ratio and aspect ratio, the natural frequency reduces, because the structure becomes softer. It considers that the effect of electric and magnetic fields is simultaneously higher than in the other cases, because the stiffness of the micro beam is enhanced. The findings of this study can be crucial in the design of the engineering and medical industries.

*** Corresponding author.**
E-mail address: *mmohammadimehr@kashanu.ac.ir*

Cite this article as:
Mokhtarian Dehkordi, B. and Mohammadimehr, M., 2026. Forced Vibration Response of a Sandwich Cantilever Nine-Layer Microbeam with Homogeneous Core Reinforced by Nanocomposite and Piezo-Magneto-Electric Layers as a Self-Sensing Mass Sensor, *Mechanics of Advanced Composite Structures*, 12(1), pp. xx-xx
https://doi.org/10.22075/MACS.2024.39315.2050

Highlights:

1- Considering a sandwich microbeam with two different lengths for the core layer and the other layers.

2- Investigating two methods, including the separation of variables method for different B.C.'s (S-S, C-S, C-C, and C-F) and Navier's method for S-S B.C.

3- Considering a nine-layer sandwich microbeam, such as a nanocomposite (two layers) and piezo-magneto-electric layers (two layers), electrode layers (four layers), and a homogeneous core.

4- Illustrating a self-sensing mass sensor at the end of the core layer.

5- Investigating the voltage, magnetic field intensity, layer thickness ratios, and CNT volume fraction.

1. Introduction

Piezo-electric sandwich microbeams have been used in micro-electro-mechanical systems (MEMS) as self-sensing mass sensors. Calibration of sensor values and parameters of sensitivity to the system makes it possible to apply micro- and nano-scale sensors. The main aspects of self-sensing mass sensors are piezoelectric microbeams, the frequency response, and the amplitude, which can be taken as measurement parameters for each microbeam oscillation. One of the most important topics related to the subject of applied physics is the design and construction of structures at micro and nano scales. In the analysis of vibrations of size-dependent beams, either in a simple or reinforced manner with carbon nanotube distribution at nano or micro scales, various numerical methods are employed. Considering different theories and boundary conditions, the effect of size and different solution methods, such as the multiscale method and the Fourier series, the problem's response is estimated analytically and approximately [1-3]. Furthermore, in the vibration analysis for single-layer or multi-layers microbeams composed of foam materials, considering added mass with theories such as modified couple stress theory and third-order shear deformation theory based on Hamilton's principle and perturbation method, it can be inferred that boundary conditions, added mass, and even electric fields are influential parameters for beams at micro and nano scales [4-5]. Recently, the vibration response analysis of sandwich beams and plates has attracted significant attention in vibration-sensitive applications. The use of advanced numerical methods, such as meshless collocation and higher-order beam theory, enables accurate investigation of free and forced vibration while providing reasonable precision with reducing of computational time. Designing sandwich structures with tailored cores, variable material distribution, and optimized geometry can achieve optimal vibration performance, favorable stiffness-to-weight ratios, and more precise responses under applied forces. Moreover, examining the effects of boundary conditions, layer thicknesses, and equivalent mechanical properties contributes to a better understanding of the dynamic behavior of these beams and can guide optimal design for high-sensitivity engineering applications. In their study, the vibration response of a self-sensing micro-sandwich beam is investigated, considering structural geometry, equivalent mechanical properties, material distribution, and various boundary conditions. The analysis encompasses the effects of geometric parameters, layer thicknesses, and material properties on natural frequencies, vibration modes, and the forced response of the beam. The results indicated that the optimization of a sandwich structure can enhance vibration performance, provide more accurate responses to external forces, and improve the precision of embedded sensors [6-8]. Another important study regarding the vibration response of beams involves topics for these structures [9]. Therefore, some studies about composite sandwich beams reinforced with a homogeneous core can investigate the vibration response and critical buckling load under various boundary conditions. The sensitivity of mechanical properties considering thermal and environmental conditions can be analyzed numerically and experimentally. These studies are not only derived from Hamilton's principle but also extracted through experimental axial tension and flexural tests based on relevant standards [10-14]. Recently, these structures have been studied using a combination of spectral geometry methods and incremental harmonic balance, taking into account nonlinear geometric factors. The mixture rule also expresses the determination of the characteristics for various parameters. The working environment can also be considered based on thermal environments through a layered coupled interlayer spring with a linear and shear layer [15-16]. Analyzing and investigating the factors affecting the sensitivity and excitability of piezoelectric microbeams, as

well as achieving maximum vibrational motion with minimal input voltage to the system for reducing power consumption and minimizing noise, are important. Piezo-electric materials serve as intelligent components employed in sensing and actuation processes essential for engineering structures. The results indicated that electrical voltage and residual stress, according to the higher-order elasticity theory, influence the dynamics of structures and play a main role in the design of controllers. The effect of the gradient index is also important for static and dynamic deformations. So far, various theories, parameters, and methods have been developed in this field, including the piezo-electric layers as sensors and actuator to control the amplitude of vibration, Euler-Bernoulli theory, differential quadrature method, dynamic flexoelectric effect, etc. [17-21]. One of the research areas in the field of sandwich beams involves the vibration and bending response analysis of multilayer composite sandwich beams with honeycomb cores. Based on the sinusoidal shear deformation theory, bending responses are analyzed simultaneously, and equilibrium equations are derived using the principle of minimum potential energy and Hamilton's principle [22]. In the vibration analysis of sandwich beams, the faces can be reinforced with graphene nanoplatelets, and to improve the accuracy of the studies, the modeling of the core and faces of the beam is performed based on the Timoshenko beam theory using Navier's method. According to the results, increasing the concentration of graphene nanoplatelets in the faces significantly enhances the natural frequency [23]. In the vibration analysis of sandwich structures, thickness stretching and size effects can also be considered according to the modified couple stress theory. Each layer in these structures may exhibit temperature-dependent mechanical properties. The proposed model, based on a higher-order shear and normal deformation theory incorporating stretching functions, offers advantages that can improve computational efficiency [24]. One of the research areas that is conducted in the field of sandwich beams is the numerical and experimental analysis of vibrations of magneto-electroelastic beams in a thermal environment. The relevant equations are extracted using the differential transformation method or radial basis functions and solved in Laplace space. Based on axial tension experiments and the mechanical properties of the elastic core, displacement and strain contours are extracted. The core can be considered as visco-elastic, electro-elastic, elastic, and electro-rheological under both static and dynamic loads. The influence of various parameters, such as spring constant, velocity ratio, volume fraction of properties, and distribution algorithm on the core is investigated [25-28]. Modeling and harvesting of vibrational energy to increase bandwidth as a mechanical amplifier, considering the geometry of devices and performance parameters, is another important topic where beams are introduced by researchers for optimization and improvement of efficiency [29-32]. In the finite element method, the mechanical and vibrational behaviors of sandwich beams are investigated, considering toughness, material properties, modal analysis, shear effects, and material gradient parameters. These studies cover beams with both constant and variable cross-sectional areas [33-36]. The impact response analysis of sandwich materials is also investigated in relation to double-curvature shells due to their unique deformation behavior and high energy absorption capacity. The properties of the materials used in the thickness direction are introduced based on volume fractions according to power and exponential laws. In this study, based on Hertz's theory and first-order shear deformation theory, an analytical model is developed to investigate the impact phenomenon. The equations of motion are derived using Hamilton's principle and then analytically analyzed using Navier's technique to assess the effects of various parameter changes, such as the volume fraction exponent, radii of principal curvatures, porosity volume fraction, and inclined angle of the core layer, on the impact response of the sandwich shell [37]. Other studies in the field of dynamic response analysis for honeycomb sandwich panels are focused on the design of three-dimensional hexagonal and concave circular honeycomb structures combined with a parallel method, as well as a hybrid parallel sinusoidal three-dimensional honeycomb structure (SPHH) with a negative Poisson's ratio. In their study, an experiment was conducted through finite element modeling (FEM) on a platform, where the experimental results showed good agreement with the FEM results [38]. Additionally, residual stresses and tensile strength in the composite faces can be investigated experimentally in such composite structures [39]. Besides structural vibrations, velocity and impact responses also play a crucial role in the appeal of these analyses in sandwich structures. Recent finite element analyses demonstrate that reinforcing the connections between the faces and the core leads to effective energy absorption by the structure. According to the findings, sandwich structures with rubber cores perform better than those with epoxy

cores, highlighting the potential of resilient sandwich structures [40].

The present study provides a comprehensive and highly detailed investigation of self-sensing sandwich microbeams, highlighting several innovative aspects that distinguish it from previous works. For the first time, the nine-layer sandwich microbeam with two different lengths for the core layer and the other layers is modeled, enabling a precise and thorough analysis of the structural vibration behavior. The inclusion of electrodes as primary layers in the piezo-magneto-electric configuration ensures a uniform electric field distribution, reduces edge stress concentration, lowers contact resistance, and enhances energy efficiency, thereby significantly improving the performance and durability of the microbeam as an approach that is not systematically addressed in prior studies. The simultaneous effects of multiple key parameters on the frequency response function amplitude are also examined, including Young's modulus to the density ratio, volume fraction and various distributions of CNT, adding mass sensor at the end core layer, input voltage, length of each layer to the length of core ratio, different boundary conditions including S-S, C-S, C-C, and C-F, material length scale parameter, and slenderness ratio. Furthermore, two methods, namely the separation of variables method for different boundary conditions (B.C.'s), including S-S, C-S, C-C, and C-F, as well as Navier's type solution method for S-S boundary condition, are employed to solve the governing equation of motion. The obtained results from both methods are compared and validated, ensuring the reliability of the findings. These innovations in a nine-layer sandwich microbeam and methodological advancements clearly demonstrate the significant contribution of this study to the design of high-performance sandwich microbeams based on a self-sensing mass sensor. On the other hand, the present study is to investigate simultaneously forced vibration response of a nine-layer sandwich microbeam with homogeneous core reinforced by nanocomposite and piezo-magneto-electric layers as a self-sensing mass sensor at the end core layer by considering two methods, including the separation of variables for different B.C.'s and Navier's method for the S-S case.

2. Modeling of a Piezo-Magneto-Electric Sandwich Microbeam

For forced vibration response and modeling of a sandwich structure, a laminated sandwich microbeam is considered, consisting of two thin composite layers and two piezo-magneto-electric layers encapsulated by two electrodes on both sides, separated by a lightweight and homogeneous material as the main layer of the sandwich microbeam (homogeneous core) (Figure 1). The length of the sandwich microbeam core (main layer), the length of the layers including the nanocomposite face sheets, piezo-magneto-electric layers, and electrodes, the total thickness of a sandwich beam, and the width of the layers are denoted by L_1, L, h, and b, respectively. The origin of the Cartesian coordinate system (zero point) is located at the bottom-left corner, and the central axis (mid-section) of the microbeam is studied, where x, z, and y represent the length, height, and width of the sandwich microbeam, respectively.

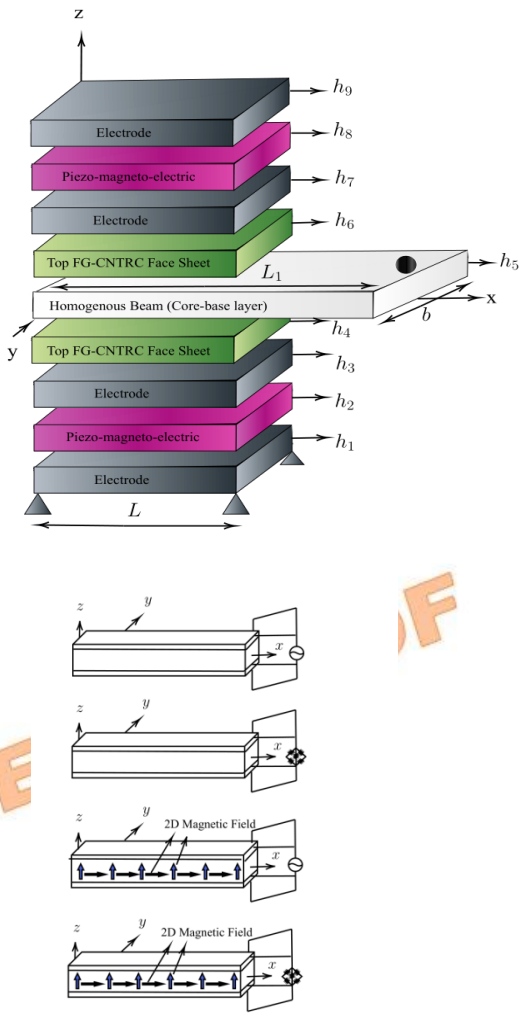

Fig 1. A schematic view of a nine-layer sandwich cantilever microbeam with a homogeneous core reinforced by a nanocomposite and two piezo-magneto-electric layers, and four electrode layers

The piezo-magneto-electric layers at the top of the microbeam can connect to the electrodes. It can be used as an actuator layer for the

sandwich microbeam (actuator layer). The bottom piezo-magneto-electric (sensing layer) is subjected to electric and magnetic fields through the electrodes. The basic constituent of the sandwich microbeam is the homogeneous core, made of pure aluminum, and the face sheets are fabricated by CNTRC in the thickness direction. Subsequently, the extended rule of mixture is presented as a suitable approach for estimating the properties of two-phase nanocomposite materials [41].

$$E_{11CNT-m} = \eta_1 V_{CNT} E_{11-CNT} + V_m E_m \quad (1)$$

where E_{11-CNT} and E_m are the elastic modulus of carbon nanotubes and the matrix, respectively. V_{CNT} and V_m stand for the volume fractions of carbon nanotubes and the matrix, respectively. It is shown through subscripts *CNT* and *m*, which are for carbon nanotubes and matrix, respectively. Similarly, the density for the CNTRC face sheets based on the mixture rule can be considered as follows [41]:

$$\rho = V_{CNT}\rho_{CNT} + V_m \rho_m \quad (2)$$

where ρ_{CNT} and ρ_m are the densities of CNT and matrix, respectively. The different distributions of CNTRC along the thickness direction of the sandwich microbeam layers are given as follows [42]:

$$FG-UD: V_{CNT} = V_{CNT}^* \quad (3)$$

$$FG-V: V_{CNT} = (1+\frac{2z}{h}) V_{CNT}^* \quad (4)$$

$$FG-O: V_{CNT} = 2(1-2\frac{|z|}{h}) V_{CNT}^* \quad (5)$$

$$FG-X: V_{CNT} = (4\frac{|z|}{h}) V_{CNT}^* \quad (6)$$

$$V_{CNT}^* = \frac{W_{CNT}}{W_{CNT} + (\rho^{CNT}/\rho^m)(1-W_{CNT})} \quad (7)$$

where V_{CNT}^* and W_{CNT} are the volume and weight fractions of the microbeam.

3. The Governing Equations of Motion for the Sandwich Microbeam

The basic relationships of the sandwich microbeam have been obtained with the following assumptions:

- It is assumed that the beam section is infinitely rigid in its own plane. Thus, there is no deformation in the plane of the cross-section. On the other hand, the cross-section of the beam remains plane to the deformed axis of the beam.

- The main layer (core) of the sandwich microbeam consists of a homogeneous and uniform material with linear elastic properties.

- Due to the adhesion and rigidity of the sandwich microbeam layers, slippage and displacement between them (composite face sheets, piezo-magneto-electric, and core) are neglected, and the stiffness and thickness of the adhesive used in bonding the layers are disregarded. The adhesives transfer all the stress properties from the piezo-magneto-electric. On the other hand, in this study, a perfect bonding assumption is adopted between all sandwich layers, including the composite face sheets, electrode layers, piezo–magneto–electric layers, and the homogeneous core. This assumption ensures that the layers behave as fully bonded layers, providing the same displacement fields for a sandwich microbeam, and enables accurate vibration analysis using classical methods, such as Navier's and separation of variables methods. However, in actual microscale fabrication, limitations such as finite adhesive thickness, material heterogeneity, micro-defects, and non-uniform bonding may introduce minor interfacial slip. These factors can have a limited effect on the local vibration response. However, the perfect bonding assumption remains a reasonable approximation for the overall dynamic behavior of the system and allows precise analysis of the global structural response within practical accuracy limits.

To derive the governing equation of motion and relevant relationships, the strain energy, including nine layers of a sandwich beam under electro-magnetic fields, is formulated as follows [3]:

$$U = \frac{1}{2}\int (\sigma_{ij}\varepsilon_{ij} + m_{ij}\chi_{ij} - D_i E_i - B_i H_i)\, dV \quad (8)$$

where σ_{ij}, ε_{ij}, m_{ij}, χ_{ij}, D_i and E_i are stress, strain, couple stress, symmetric rotation tensors, electric displacement, and electric field, respectively. U is the strain energy. Also, the parameters B_i and H_i represent the effects of magnetic displacement and magnetic field, respectively. This equation indicates that the system's strain energy is not limited to mechanical deformation alone, but also involves electric and magnetic fields. The strain and stress components represent the stiffness and mechanical resistance of the structure, determining how the microcantilever responds to deformation and vibration. The couple stress and symmetric rotation components account

for the rotational effects of the layers, controlling the distribution of stress and strain at micro scales.

The electrical and magnetic components have a direct impact on the amplitude and sensitivity of the microcantilever's response, showing how electrical excitation and magnetic fields can modulate the system's dynamic behavior. In other words, the energy stored in the structure results from the simultaneous interaction of mechanical, electrical, and magnetic contributions, each exerting its specific influence on vibration and sensor sensitivity.

The kinematic equations based on modified couple stress theory at the micro scale using linear displacements are defined as follows [58]:

$$\varepsilon_{ij} = \frac{1}{2}(u_{i,j} + u_{j,i}),\ \varepsilon_{11} = -z\frac{\partial^2 w_0}{\partial x^2},\ \varepsilon_{13} = 0 \quad (9)$$

$$\chi_{ij} = \frac{1}{2}(\theta_{i,j} + \theta_{j,i}),\ \chi_{12} = -\frac{1}{2}\frac{\partial^2 w_0}{\partial x^2} \quad (10)$$

$$m_{12} = 2\mu l_m^2 \chi_{12} \quad (11)$$

where w_0, μ, and l_m are the transverse displacement, shear modulus, and the material length scale parameter. Also, θ_i shows the components of the rotation vector θ. In Euler-Bernoulli beam theory, there is only normal strain in the x direction, and the shear strain is zero. The transverse displacement reflects the bending of the microbeam. The material length scale parameter is taken into account at the micro scale, ensuring that the structural response is accurately captured at micro dimensions.

The electric and magnetic potential fields and displacements for piezo-magneto-electric materials are also given by [59]:

$$E_1 = -\frac{\partial \phi}{\partial x},\ E_3 = -\frac{\partial \phi}{\partial z} \quad (12)$$

$$H_1 = -\frac{\partial \psi}{\partial x},\ H_3 = -\frac{\partial \psi}{\partial z} \quad (13)$$

$$D_1 = e_{15}\varepsilon_{13} + \eta_{11}E_1 + g_{11}H_1 \quad (14)$$

$$D_3 = e_{31}\varepsilon_{11} + \eta_{33}E_3 + g_{33}H_3 \quad (15)$$

$$B_1 = q_{15}\varepsilon_{13} + \mu_{11}H_1 + g_{11}E_1 \quad (16)$$

$$B_3 = q_{31}\varepsilon_{11} + \mu_{33}H_3 + g_{33}E_3 \quad (17)$$

where ϕ, and (e_{15}, e_{31}, η_{11} and η_{33}) are the electric potential, and the properties of piezo-magneto-electric materials. E_1 and E_3 are the electric fields in x and z directions; also, D_1 and D_3 denote the electric displacements. Similarly ψ and (q_{15}, q_{31}, μ_{11} and μ_{33}) are the magnetic potential and magnetic constants, respectively. Also, H_1 and H_3 are the magnetic fields in the x and z directions, and B_1 and B_3 are the magnetic displacements. These relations show how electric and magnetic fields interact with displacements in piezo-magneto-electric materials. The electric potential and material constants determine how applying an electric field distributes the electric potential and induces structural displacements. Similarly, the magnetic potential and magnetic constants govern how an applied magnetic field affects displacements and magnetic potential within the material. These interactions directly influence the vibrational response of the microbeam, including its vibration amplitude and sensitivity to environmental changes, highlighting the coupling between mechanics, electricity, and magnetism in the system.

According to Eq. (9) for the Euler-Bernoulli beam, in Eqs. (14) and (16), the shear strain is equal to zero ($\varepsilon_{13} = 0$). Thus, Eqs. (14) and (16) are rewritten as:

$$D_1 = \eta_{11}E_1 + g_{11}H_1 \quad (18)$$

$$B_1 = \mu_{11}H_1 + g_{11}E_1 \quad (19)$$

The resultant bending moment M_x for the Euler-Bernoulli sandwich beam, by considering nine layers is defined as follows [61-63]:

$$z_n = \frac{\sum_{k=1}^{n} E^{(K)} w^{(K)} h^{(K)} \left(\sum_{j=1}^{k-1} h^{(j)} + \frac{h^{(k)}}{2}\right)}{\sum_{k=1}^{n} E^{(k)} w^{(k)} h^{(k)}} \quad (20)$$

$$M_x = \sum_{k=1}^{n} \int_{z_u + \sum_{j=1}^{k-1} h^{(j)}}^{z_u + \sum_{j=1}^{k} h^{(j)}} \sigma_x^{(k)} .z\, dz \quad (21)$$

By substituting relations (9), (12), and (13) into relation (8), the following form based on the variational method can be obtained as follows:

$$\begin{aligned}\delta U = &-\int M_x \delta \frac{\partial^2 w_0}{\partial x^2} dA - \frac{1}{2}\int M_{xy}^{(0)} \delta \frac{\partial^2 w_0}{\partial x^2} dA \\ &+ \int D_1 \delta \frac{\partial \phi}{\partial x} dV + \int D_3 \delta \frac{\partial \phi}{\partial z} dV \\ &+ \int B_1 \delta \frac{\partial \psi}{\partial x} dV + \int B_3 \delta \frac{\partial \psi}{\partial z} dV\end{aligned} \quad (22)$$

where $M_{xy}^{(0)}$ is related to the effect of the material length scale parameter that is defined as follows:

$$M_0 = \sum_{k=1}^{n} \int_{z_u + \sum_{j=1}^{k-1} h^{(j)}}^{z_u + \sum_{j=1}^{k} h^{(j)}} m_{12}^{(k)} z^0 dz \quad (23)$$

After applying the variational method in equation (22), the final equation is considered in the following form:

$$\delta U = -\int \frac{\partial^2 M_x}{\partial x^2}(\delta w_0)dA - \frac{1}{2}\int \frac{\partial^2 M_{xy}^{(0)}}{\partial x^2}(\delta w_0)dA - \int \frac{\partial D_1}{\partial x}(\delta\phi)dV - \int \frac{\partial D_3}{\partial z}(\delta\phi)dV - \int \frac{\partial B_1}{\partial x}(\delta\psi)dV - \int \frac{\partial B_3}{\partial z}(\delta\psi)dV \quad (24)$$

The above equation represents physically the amount of elastic energy stored in the structure and serves as a measure of its stiffness or flexibility. Variations under different conditions—such as changes in layer thickness or ratios, and applied electric and magnetic fields—indicate how the structure alters its frequency response function (FRF) and how input energy is converted into mechanical strain. Also, an increase reflects a stiffer structure, while a decrease indicates greater flexibility, both of which are directly related to changes in the natural frequency and FRF amplitude.

General equations for determining the kinetic energy of the sandwich micro cantilever beam are written as follows [43-44]:

$$T = \int \frac{1}{2}\rho\left(\left(\frac{\partial U}{\partial t}\right)^2 + \left(\frac{\partial V}{\partial t}\right)^2 + \left(\frac{\partial W}{\partial t}\right)^2\right)dV \quad (25)$$

$$\delta T = \int \rho\left(\left(z^2 \frac{\partial^2 w_0}{\partial x \partial t}\right)\delta\left(\frac{\partial^2 w_0}{\partial x \partial t}\right) + \left(\frac{\partial w_0}{\partial t}\right)\delta\left(\frac{\partial w_0}{\partial t}\right)\right)dV \quad (26)$$

where T and ρ are the kinetic energy and the density of the microbeam, respectively. After applying the variational method in equation (26), the following equation can be obtained as follows:

$$\delta T = \int \left(I^{(2)}\frac{\partial^4 w_0}{\partial x^2 \partial t^2}\right)(\delta w_0) - I^{(0)}\frac{\partial^2 w_0}{\partial t^2}(\delta w_0) - M_e \frac{\partial^2 w_0(x,t)}{\partial t^2}\delta(x - L_1)(\delta w_0))\,dA \quad (27)$$

where M_e is the concentrated mass at the end of the core layer from the sandwich microbeam.

δT represents the variations in the kinetic energy of the system, which are directly related to the velocity of the layer motions and the mass of the structure. This quantity indicates how the mass distribution and the density of the layers, along with the vibrational motion of the microcantilever, influence the dynamic response. When δT is examined under different conditions, such as changes in layer thickness, thickness ratios, or the addition of the concentrated mass at the end of the microbeam, it is possible to observe how the kinetic energy is distributed within the system and which parts of the structure contribute most to the motion.

Also, $I^{(0)}$ and $I^{(2)}$ are the mass inertia for a sandwich microcantilever beam with nine layers, including a piezo-magneto-electric layer between two electrode layers, CNTRC in the top and bottom core, and a homogeneous core, which are given as follows:

$$I^{(0)} = \sum_{k=1}^{n}\int_{z_u+\sum_{j=1}^{k-1}h^{(j)}}^{z_u+\sum_{j=1}^{k}h^{(j)}} \rho^{(k)}.z^0.dz \quad (28a)$$

$$I^{(2)} = \sum_{k=1}^{n}\int_{z_u+\sum_{j=1}^{k-1}h^{(j)}}^{z_u+\sum_{j=1}^{k}h^{(j)}} \rho^{(k)}.z^2.dz \quad (28b)$$

The variation of the external work due to pre-stress load under piezo-electro-magnetic fields and external voltage is considered as follows:

$$\delta W_{ext} = -\int (N_{x0}\frac{\partial^2 w_0(x,t)}{\partial x^2} + V_0 \sin\Omega t)\delta w_0\,dA \quad (29)$$

where N_{x0} denotes the pre-stress load under piezo-electro-magnetic fields and V_0 is the external voltage.

The dynamic equations of the sandwich microcantilever beam are extracted based on Hamilton's principle as follows [45]:

$$\int \delta\prod dt = 0, \prod = T - (U - W_{ext}) \quad (30)$$

where T, U, and W_{ext} represent the kinetic energy, the strain energy, and the external work, respectively.

Hamilton's principle states that the motion and dynamic response of a system are such that the difference between the kinetic energy and the strain energy is minimized over time. When δT, δU, and δW_{ext} are substituted into the Hamiltonian integral, the researchers are essentially examining how the kinetic energy resulting from the motion of the layers and the strain energy arising from the deformation of the structure interact to determine the system's dynamic behavior. This physical approach demonstrates that the natural frequencies and FRF amplitudes of the microbeam are shaped by the balance between the strain energy stored in the layers and the kinetic energy associated with the motion of the various layer masses.

By substituting equations (24) and (27) into Hamilton's principle (Eq. (30)), the differential equation is derived as:

$$\iint (I^{(2)} \frac{\partial^4 w_0}{\partial x^2 \partial t^2}(\delta w_0) - I^{(0)} \frac{\partial^2 w_0}{\partial t^2}(\delta w_0) - M_e \frac{\partial^2 w_0(x,t)}{\partial t^2}\delta(x - L_1)(\delta w_0) - N_{x0} \frac{\partial^2 w_0}{\partial x^2}(\delta w_0) - V_0 \sin\Omega t\ \delta w_0 + \frac{\partial^2 M_x}{\partial x^2}(\delta w_0) + \frac{1}{2}\frac{\partial^2 M_{xy}^{(0)}}{\partial x^2}(\delta w_0) + \frac{\partial \bar{D}_1}{\partial x}(\delta\phi) + \bar{D}_3(\delta\phi) + \frac{\partial \bar{B}_1}{\partial x}(\delta\psi) + \bar{B}_3(\delta\psi))dtdA = 0 \quad (31)$$

By substituting the kinetic energy, strain energy, and the external work into Hamilton's principle, the governing equation of the motion for the sandwich micro-cantilever beam is expressed as follows:

$$(\delta w_0): \frac{\partial^2 M_x}{\partial x^2} + \frac{1}{2}\frac{\partial^2 M_{xy}^{(0)}}{\partial x^2} - N_{x0}\frac{\partial^2 w_0}{\partial x^2} - I^{(0)}\frac{\partial^2 w_0}{\partial t^2} + I^{(2)}\frac{\partial^4 w_0}{\partial x^2 \partial t^2} - \int M_e \frac{\partial^2 w_0(x,t)}{\partial t^2}\delta(x - L_1)dx = V_0 \sin\Omega t \quad (32)$$

$$(\delta\phi): \frac{\partial \bar{D}_1}{\partial x} + \bar{D}_3 = 0 \quad (33)$$

$$(\delta\psi): \frac{\partial \bar{B}_1}{\partial x} + \bar{B}_3 = 0 \quad (34)$$

where [60]:

$$\bar{D}_1 = \int D_1 dz\ , \bar{D}_3 = \int \frac{\partial D_3}{\partial z}dz \quad (35)$$

$$\bar{B}_1 = \int B_1 dz\ , \bar{B}_3 = \int \frac{\partial B_3}{\partial z}dz \quad (36)$$

The resultant bending moment is written as follows:

$$M_x = \int_{-\frac{h}{2}}^{+\frac{h}{2}} (-Ez^2 \frac{\partial^2 w_0}{\partial x^2} - z\, e_{13} E_3 - z\, q_{13} H_3)dz = -A^{(2)}\frac{\partial^2 w_0}{\partial x^2} + e_{13}\bar{\phi}_3 + q_{13}\bar{\psi}_3 \quad (37)$$

where

$$\bar{\phi}_3 = \int \frac{\partial \phi}{\partial z} z\ dz = B^{(1)}\phi_{(x,t)} \quad (38)$$

$$\bar{\psi}_3 = \int \frac{\partial \psi}{\partial z} z\ dz = B^{(1)}\psi_{(x,t)} \quad (39)$$

Also, the parameter $A^{(2)}$ is defined as follows:

$$A^{(2)} = \int Ez^2 dz \quad (40)$$

The value of $A^{(2)}$ for a nine-layer sandwich microcantilever beam, including piezo-magneto-electric layers between electrode layers, nanocomposite layers, and a homogeneous core, is defined as follows:

$$A^{(2)} = \sum_{k=1}^{n} \int_{z_u + \sum_{j=1}^{k-1} h^{(j)}}^{z_u + \sum_{j=1}^{k} h^{(j)}} E^{(k)} . z^2 . dz \quad (41)$$

Additionally, by substituting Eq. (10) into Eq. (11), the following equation is obtained as [59]:

$$m_{12} = -\mu l_m^2 \frac{\partial^2 w_0}{\partial x^2} \quad (42)$$

Therefore, parameters $B^{(0)}$ and $M_{xy}^{(0)}$ are defined as follows:

$$B^{(0)} = \int \mu l_m^2 dz \quad (43)$$

$$M_{xy}^{(0)} = \int m_{12} dz = \int -\mu l_m^2 \frac{\partial^2 w_0}{\partial x^2} dz = -B^{(0)}\frac{\partial^2 w_0}{\partial x^2} \quad (44)$$

where $B^{(0)}$ for nine-layer sandwich beam is considered as follows:

$$B^{(0)} = \sum_{k=1}^{n} l_m^2 \int_{z_u + \sum_{j=1}^{k-1} h^{(j)}}^{z_u + \sum_{j=1}^{k} h^{(j)}} \mu^{(k)} z^0 dz \quad (45)$$

Therefore, the bending moment is rewritten as follows:

$$M_x = -A^{(2)}\frac{\partial^2 w_0}{\partial x^2} + e_{13} B^{(1)}\phi_{(x,t)} + q_{13} B^{(1)}\psi_{(x,t)} \quad (46)$$

By substituting equations (42) and (44) into equation (32), based on Hamilton's principle, the governing equation of motion for the sandwich microcantilever beam is obtained as follows:

$$(\delta w_0): -A^{(2)}\frac{\partial^4 w_0}{\partial x^4}-\frac{1}{2}B^{(0)}\frac{\partial^4 w_0}{\partial x^4}$$
$$-N_{x0}\frac{\partial^2 w_0}{\partial x^2}$$
$$+e_{13}B^{(1)}\frac{\partial^2 \phi_{(x,t)}}{\partial x^2}+q_{13}B^{(1)}\frac{\partial^2 \psi_{(x,t)}}{\partial x^2}$$
$$-I^{(0)}\frac{\partial^2 w_0}{\partial t^2}+I^{(2)}\frac{\partial^4 w_0}{\partial x^2 \partial t^2}$$
$$-\int M_e \frac{\partial^2 w_0(x,t)}{\partial t^2}\delta(x-L_1)dx$$
$$=V_0 \sin\Omega t \quad (47)$$

$$(\delta\phi): \frac{\partial \bar{D}_1}{\partial x}+\bar{D}_3=0 \quad (48)$$

$$(\delta\phi): \frac{\partial \bar{B}_1}{\partial x}+\bar{B}_3=0 \quad (49)$$

Considering relations (35) and (36), the governing equations of motion (Eqs. (48) and (49)) are rewritten as follows:

$$(\delta\phi): \eta_{11}\alpha_1^{(C)}\frac{\partial^2 \phi_{(x,t)}}{\partial x^2}+g_{11}\alpha_1^{(C)}\frac{\partial^2 \psi_{(x,t)}}{\partial x^2}$$
$$-e_{13}\alpha_1^{(0)}\frac{\partial^2 w_0}{\partial x^2}-\eta_{33}\phi_{(x,t)}(\frac{\pi}{h})^2\alpha_1^{(C)} \quad (50)$$
$$-g_{33}\psi_{(x,t)}(\frac{\pi}{h})^2\alpha_1^{(C)}=0$$

$$(\delta\psi): \mu_{11}\alpha_1^{(C)}\frac{\partial^2 \psi_{(x,t)}}{\partial x^2}+g_{11}\alpha_1^{(C)}\frac{\partial^2 \phi_{(x,t)}}{\partial x^2}$$
$$-q_{13}\alpha_1^{(0)}\frac{\partial^2 w_0}{\partial x^2}-\mu_{33}\psi_{(x,t)}(\frac{\pi}{h})^2\alpha_1^{(C)} \quad (51)$$
$$-g_{33}\phi_{(x,t)}(\frac{\pi}{h})^2\alpha_1^{(C)}=0$$

4. Solution Method

In relation to the scientific background of this research, dynamic modeling for forced vibration of a sandwich microbeam under the influence of the electric and magnetic fields is conducted. Using the energy method and Hamilton's principle, the governing equations of motion for the microbeam are extracted. Then, these equations are solved using separation of variables to determine the natural frequencies and vibration modes of the system. The significance of this model lies in its ability to predict the dynamic behavior of the microbeam under various boundary conditions and to optimize the design of similar structures. The results obtained from this model can be utilized in the design of sensors, actuators, and smart materials with wide-ranging applications in various industries. This knowledge provides an opportunity to enhance existing theories and offers more accurate models for predicting the behavior of these structures. In industry, mathematical models are employed to optimize manufacturing processes, design new products, optimize structural designs, extend their lifespan, and reduce costs. From an industrial perspective, the results can be applicable in various sectors, such as aerospace, automotive, electronics, and medical equipment manufacturing. For instance, this model can be used for the design of more precise vibration sensors and micro-electromechanical actuators.

4.1. Navier's Method

In this section, Navier's solution method is examined to solve the governing equation of motion under simply supported boundary conditions. Accordingly, the transverse displacement and electric and magnetic potential functions are expressed as follows:

$$W_{(x,t)}=\sum W_m \sin(\frac{m\pi x}{l})\, e^{i\omega_m t}$$
$$\phi_{(x,t)}=\sum \phi_m \sin(\frac{m\pi x}{l})\, e^{i\omega_m t} \quad (52)$$
$$\psi_{(x,t)}=\sum \psi_m \sin(\frac{m\pi x}{l})\, e^{i\omega_m t}$$

where ω_m is the natural frequency of the structure. Also W_m , ϕ_m and ψ_m are unknown coefficients. By substituting equations (52) into (47), (50), and (51), the mass and stiffness matrices are defined as follows:

Stiffness matrix:

$$[K]=\begin{bmatrix} K_{11} & K_{12} & K_{13} \\ K_{21} & K_{22} & K_{23} \\ K_{31} & K_{32} & K_{33} \end{bmatrix}$$

$$K_{11}=A^{(2)}(\frac{m\pi}{l})^4+\frac{1}{2}B^{(0)}(\frac{m\pi}{l})^4$$
$$-N_{x0}(\frac{m\pi}{l})^2$$

$$K_{12}=e_{13}B^{(1)}(\frac{m\pi}{l})^2$$

$$K_{13}=q_{13}B^{(1)}(\frac{m\pi}{l})^2 \quad (53)$$

$$K_{21}=e_{13}\alpha_1^{(0)}(\frac{m\pi}{l})^2$$

$$K_{22}=-\eta_{11}\alpha_1^{(C)}(\frac{m\pi}{l})^2-\eta_{33}(\frac{\pi}{h})^2\alpha_1^{(C)}$$

$$K_{23}=-g_{11}\alpha_1^{(C)}(\frac{m\pi}{l})^2-g_{33}(\frac{\pi}{h})^2\alpha_1^{(C)}$$

$$K_{31}=q_{13}\alpha_1^{(0)}(\frac{m\pi}{l})^2$$

$$K_{32}=-g_{11}\alpha_1^{(C)}(\frac{m\pi}{l})^2-g_{33}(\frac{\pi}{h})^2\alpha_1^{(C)}$$

$$K_{33}=-\mu_{11}\alpha_1^{(C)}(\frac{m\pi}{l})^2-\mu_{33}(\frac{\pi}{h})^2\alpha_1^{(C)}$$

Mass matrix:

$$[M]=\begin{bmatrix} M_{11} & M_{12} & M_{13} \\ M_{21} & M_{22} & M_{23} \\ M_{31} & M_{32} & M_{33} \end{bmatrix}$$

$$M_{11}=I^{(2)}(\frac{m\pi}{l})^2+I^{(0)}+M_e\omega^2\sin(\frac{n\pi L_1}{l}) \quad (54)$$

$$M_{12}=M_{13}=M_{21}=M_{22}=0$$

$$M_{23}=M_{31}=M_{32}=M_{33}=0$$

The added mass at the end of the core layer for the sandwich microcantilever beam is represented by M_e. The natural frequencies of the sandwich microbeam for free vibration are obtained using the stiffness and the mass matrices [4]:

$$\det([K]-\omega_n^2[M])=0 \quad (55)$$

In this section, to validate the Navier solution method, the method of separation of variables solution is examined for solving the governing equation of motion under various boundary conditions. Therefore, to solve the differential equation of motion (Equation 47) and utilize the pertinent boundary and continuity conditions, the method of separation of variables is employed to determine the natural frequencies of the microcantilever Euler-Bernoulli sandwich beam, including a homogeneous core, FG-CNTRC layers at the top and bottom of the core, and piezo-magneto-electric layers between the electrode layers.

4.2. Separation of Variables Method

Hence, based on the separation of variables method, the deflection of the cantilever micro beam at any point is defined as follows:

$$w_{(x,t)}=Ae^{rx}e^{i\omega t} \quad (56)$$

where Ae^{rx} and $e^{i\omega t}$ represent the term for microcantilever deflection, by performing differentiation operations.

In this article, due to the consideration of micro dimensions (length, width, and thickness), the small-scale effect is addressed, and the modified coupled stress theory (MCST) is used to study this effect. Another reason for using this theory is that it provides greater accuracy in analyzing stresses and strains in materials. This theory allows engineers to create better designs for structures, leading to a more precise modeling of material behavior under real conditions. Additionally, the use of this theory enables them to align their designs and analyses with recognized and advanced industry standards. By substituting equation (56) into equation (47) for the sandwich microbeam and considering the small-scale parameter (MCST theory), electric field, and magnetic field, the roots of the differential equation (natural frequencies of the system) are determined as [43]:

$$-I^{(0)}Ae^{rx}e^{i\omega t}(i\omega)^2$$
$$+I^{(2)}Ae^{rx}e^{i\omega t}r^2(i\omega)^2$$
$$-A^{(2)}Ae^{rx}e^{i\omega t}r^4$$
$$-\frac{1}{2}B^{(0)}Ae^{rx}e^{i\omega t}r^4 \quad (57)$$
$$+e_{13}B^{(1)}y_5r^2Ae^{rx}e^{i\omega t}$$
$$+q_{13}B^{(1)}x_5r^2Ae^{rx}e^{i\omega t}=0$$

By simplifying equation (57), it can be written as:

$$(-A^{(2)}-\frac{1}{2}B^{(0)})r^4 +(e_{13}B^{(1)}y_5+q_{13}B^{(1)}x_5-I^{(2)}\omega^2)r^2 +I^{(0)}\omega^2=0 \quad (58)$$

where the values of r_1, r_2, r_3, and r_4 are the roots of the differential equation (natural frequencies of the system) that is shown in Appendix A.

The boundary conditions, continuity considerations, and electric boundary conditions, considering the geometric discontinuities and added mass at the end of the microcantilever for a sandwich beam with nine layers, are considered as follows [46]:

$$w_{(0,t)}=0\ , EI\frac{\partial^2 w}{\partial x^2}_{(0,t)}=0$$

$$w_{(L,t)}=0\ , EI\frac{\partial^2 w}{\partial x^2}_{(L,t)}=0 \quad \text{for S-S} \quad (59a)$$

$$w_{(0,t)}=0\ , \frac{\partial w}{\partial x}_{(0,t)}=0$$

$$w_{(L,t)}=0\ , \frac{\partial w}{\partial x}_{(L,t)}=0 \quad \text{for C-C} \quad (59b)$$

$$w_{(0,t)}=0\ , \frac{\partial w}{\partial x}_{(0,t)}=0$$

$$EI\frac{\partial^2 w}{\partial x^2}_{(L,t)}=0\ , EI\frac{\partial^3 w}{\partial x^3}_{(L,t)}=0 \quad (59c)$$

for C-F

$$w_{1n(L_1^-,t)}=w_{2n(L_1^+,t)}\ ,$$

$$\frac{\partial w_{1n}}{\partial x}_{(L_1^-,t)}=\frac{\partial w_{2n}}{\partial x}_{(L_1^+,t)} \quad (60)$$

Boundary conditions play a crucial role in determining the dynamic behavior of the microbeam, as they define how the ends and layers of the structure are constrained or allowed to move. From a physical perspective, boundary conditions indicate which points experience higher kinetic and strain energy and how forces and deformations are distributed along the structure. For instance, a clamped end restricts both translational and rotational motion, resulting in higher effective stiffness and increasing the natural frequencies. In contrast, a free end allows greater movement and larger FRF amplitudes. This information provides a fundamental basis for the optimal design of microscale structures and for predicting their behavior in various applications.

Considering the geometric discontinuities in the sandwich microcantilever beam as depicted in Figure 1, and due to the presence of composite layers (the length L), piezo-magneto-electric layers (the length L) between two electrode layers (the length L), and the main (core) layer (the length L_1), various parts of the sandwich micro cantilever are defined different shape functions as follows [47]:

$$w_{(x)}=A_1\sinh\alpha_1 x+A_2\cosh\alpha_1 x +A_3\sin\alpha_2 x+A_4\cos\alpha_2 x\ ,\ 0\langle x\langle L_1 \quad (61)$$

$$w_{(x)}=B_1\sinh\alpha_1 x+B_2\cosh\alpha_1 x +B_3\sin\alpha_2 x+B_4\cos\alpha_2 x\ ,\ L_1\langle x\langle L \quad (62)$$

where A_1 , A_2 , A_3 , A_4 , B_2 , B_3 , B_4 , α_1 and α_2 are unknown parameters, determined based on boundary and continuity conditions, for the differential equation governing the motion.

The values of α_1 and α_2 by considering the effect of the small-scale parameter, are obtained as follows:

$$\alpha_1=\sqrt{\frac{I^{(0)}\omega^2}{(e_{13}B^{(1)}y_5+q_{13}B^{(1)}x_5-I^{(2)}\omega^2)}} \quad (63)$$

$$\alpha_2=\sqrt{\frac{(e_{13}B^{(1)}y_5+q_{13}B^{(1)}x_5-I^{(2)}\omega^2)}{(-A^{(2)}-\frac{1}{2}B^{(0)})}+\frac{I^{(0)}\omega^2}{(e_{13}B^{(1)}y_5+q_{13}B^{(1)}x_5-I^{(2)}\omega^2)}}$$

Therefore, the characteristic equation for vibration analysis of a sandwich beam is considered as follows [47]:

$$[J][A_1A_2A_3A_4B_1B_2B_3B_4]^T=0 \quad (64)$$

where the Jacobian matrix (J) is based on the aforementioned shape functions, eigenvalue equation, C-C, S-S, C-S, and C-F boundary conditions, and related continuity is expressed in Appendix B.

The natural frequencies of the sandwich microcantilever beam can be calculated using the determinant of [J]=0. The differential equations of motion based on the orthogonality theorem are considered as follows [48- 49]:

$$\ddot{q}_n + \omega_n^2 q_n + \sum_{m=1}^{\infty} c_{nm}\dot{q}_n - \gamma_n p(t) = 0 \quad (65)$$

where q_n, ω_n, c_{nm}, and $p(t)$ represent the generalized coordinates, natural frequency, intrinsic damping of the microbeam, and input voltage to the piezo-magneto-electric layer, respectively.

5. Results and Discussion

In this section, numerical results for determining frequencies and amplitude from the piezo-magneto-electric layers of the sandwich microcantilever beam, including a homogeneous core, nano composite layer, and piezo-magneto-electric layers between electrodes under relevant boundary and continuity conditions due to exposure to an electric and magnetic field, are presented. The material properties for the homogeneous aluminum or gold for the core (fifth layer) of a sandwich microcantilever beam are considered as follows [51]:

$$E_{Al} = 70GPa,\ \rho_{Al} = 2780kg/m^3 \quad (66)$$
$$E_{Au} = 79GPa,\ \rho_{Au} = 19300kg/m^3$$

The material properties for the matrix of nano composite layers of the sandwich microcantilever beam are written as follows [52]:

$$E_m = 2.5GPa,\ \rho_m = 1190kg/m^3 \quad (67)$$

The upper index m and c in equations (66) and (67) represent the characteristics of the core and the matrix in the nano composite layer of the microcantilever sandwich structure, respectively. The properties of CNTRC layers as reinforcement of composite layers are assumed as follows [53]:

$$E_{11-CNT} = 600GPa,\ \rho_{CNT} = 1400kg/m^3 \quad (68)$$

The values of CNTRC volume fraction and efficiency parameters for three numerical values are considered as [53].

The mechanical properties of the piezo-magneto-electric layers, including PZT-4 or Zn, and electrodes, such as Ti or Cu, are also defined as follows [47]:

Electrodes :

$$E_{Ti} = 110GPa,\ \rho_{Ti} = 4540kg/m^3,$$
$$E_{Cu} = 117GPa,\ \rho_{Cu} = 8940kg/m^3, \quad (69)$$

Piezo − magneto − electric :

$$E_{PZT\,4} = 81.3GPa,\ \rho_{PZT\,4} = 7000kg/m^3$$
$$E_{Zn} = 108GPa,\ \rho_{Zn} = 7000kg/m^3$$

Furthermore, the geometric dimensions of the sandwich microbeam are defined as follows:

$$H = 10(\mu m),\ L/L_1 = 0.6,$$
$$L/H = 10,\ W = 20(\mu m) \quad (70)$$
$$h_c = 0.6H,\ h = 0.05H$$

Additionally, the properties and constants related to the piezo-magneto-electric layers for PZT-4 are presented as follows [64]:

$$e_{31} = -7.54\ (C/m^2), \quad (71)$$
$$q_{31} = 89.23(N/Am)$$
$$\eta_{11} = 5.64\times10^{-9}\ (Ns/CV),$$
$$\eta_{33} = 6.75\times10^{-9}\ (Ns/CV)$$
$$\mu_{11} = -297\times10^{-6}\ (Ns^2/C^2),$$
$$\mu_{33} = 84.07\times10^{-6}\ (Ns^2/C^2)$$
$$g_{11} = 5.367\times10^{-12}\ (Ns/CV),$$
$$g_{33} = 17802.64\times10^{-12}\ (Ns/CV)$$

The results of the present research are compared and examined with the results obtained from other articles. In this study, the non-dimensional frequency parameter for the microcantilever sandwich is defined as follows [4]:

$$\bar{\omega} = \omega L^2\sqrt{\frac{\rho A}{EI}} \quad (72)$$

where $\bar{\omega}$ represents the non-dimensional frequency. Tables 1 and 2 demonstrate the effect of the length-to-thickness ratio and the CNTRC volume fraction, and the efficiency coefficient on the natural frequency of the sandwich microcantilever in the first three vibration modes. It is shown that with increasing of aspect ratio, the natural frequency decreases, because the structure becomes softer; while for volume fraction is vice versa. On the other hand, the increase in the volume fraction leads to enhance the stiffness of the structure, and then the natural frequencies increase.

Table 1. The natural frequency of the sandwich microbeam for various aspect ratios and $V_{cnt} = 0.12$ In the first three oscillation modes

L/H	First frequency (KHz)	Second frequency (KHz)	Third frequency (KHz)
10	5.4467e+03	2.0226e+04	4.1031e+04
14	2.8160e+03	1.0819e+04	2.2903+04
18	1.7130e+03	6.6826e+03	1.4459e+04

Table 2. The natural frequency of the sandwich microbeam for various volume fractions of CNTRC and L/H=10 in the first three oscillation modes

V_{cnt} %	η_1	First frequency (KHz)	Second frequency (KHz)	Third frequency (KHz)
12	1.2833	5.4467e+03	2.0226e+04	4.1031e+04
17	1.3414	5.6104e+03	2.0834e+04	4.2264e+04
28	1.3238	5.9545e+03	2.2112e+04	4.4857e+04

In Table 3, the obtained results of the microbeam for different aspect ratios in the first two oscillations, with the other reference Zari et al. [4] and Santos and Reddy [54], are compared. It is shown that there is good agreement between them. It is seen that as the aspect ratio increases, the errors reduce. The difference between the present work and other literature [4,54] becomes 3.45% and 4.69%, for aspect ratio 5, respectively. The displacement fields for the literature are third-order shear deformation beam theory and Timoshenko beam theory, that there are the normal and shear strains, while the present study considers the classical beam theory in which there is only normal strain. Thus, it is shown that with increasing of aspect ratio (L/H>=10), the difference between them is negligible.

Table 3. Dimensionless natural frequency for a sandwich microbeam $(\bar{\omega} = \omega L^2 \sqrt{\frac{I^{(0)}}{EI}})$ [4, 54]

L/H	Present study	Zari et al. [4]	Santos and Reddy [54]	Error1 (%)	Error2 (%)
5	1.2833	9.27	9.39	3.45	4.69
10	1.3414	9.70	9.74	0.10	0.31

In Table 4, the obtained results to solve the governing equation of the motion for the sandwich microbeam in the first oscillatory mode using the Navier method are compared with the separation of variables method. Based on the results, there is good agreement between the findings.

Table 4. Comparison of the natural frequencies for a sandwich microbeam using Navier's method and the separation of variables method

L/H	Navier's method	Separation of variable method	Error (%)
10	5.4467e+03	5.4478e+03	0.02
14	2.8160e+03	2.8170e+03	0.03
18	1.7130e+03	1.7188e+03	0.33

Table 5 shows a comparison of the first natural frequency for the sandwich microbeams for a) various m_e, b) various core, c)various L_1/H, d)various L/L_1, e)various lm, f) various h_c/H. It is shown from Table 5a that by increasing the values of the added mass from 0.001 to 0.01 and 0.05 microgram, the first natural frequency decreases 65.1% and 84.25%, respectively. It is depicted from Table 5b that by decreasing E/ρ from Al to Ti and Au, the first natural frequency reduces from 15.21% and 36.18%, respectively. It is illustrated from Table 5c that by increasing from 10 to 15 and 20, the first natural frequency decreases from 55.08% and 74.64%, respectively. It is observed from Table 5d that by increasing from 0.6 to 0.8 and 1, the first natural frequency decreases from 43.28% and 63.56%, respectively. It is shown from Table 5e that by considering the material length scale parameter, the first three natural frequency increases 137.9%. It is shown from Table 5f that by enhancing h_c/H from 0.6 to 0.8 and 0.9, the first natural frequency increases 16.1% and 28.5%, respectively.

Table 5. Comparison of the natural frequencies for the sandwich microbeam for a) various m_e b) various core c)various L_1/H d)various L/L_1 e)various lm f) various h_c/H

a)

Me(μgr)	The first frequency	(%)
0.001	7.0856 e+02	-
0.01	2.4707e+02	-65.1
0.05	1.1157e+02	-84.25

b)

Type of core	The first frequency	(%)
Al	4.3775 e+03	-
Ti	3.7116e+03	-15.21
Au	2.7938e+03	-36.18

c)

L1/H	The first frequency	(%)
10	4.3775 e+03	-
15	1.9662e+03	-55.08
20	1.1101e+03	-74.64

d)

L/ L1	The first frequency	(%)
0.6	4.3775 e+03	-
0.8	2.4828e+03	-43.28
1	1.5952e+03	-63.56

e)

Lm(μm)	The first frequency	(%)
0	0.5447 e+04	-
17.6	1.2959e+04	+137.9

f)

hc/h	The first frequency	(%)
0.6	4.2865 e+03	-
0.8	4.9787e+03	+16.1
0.9	5.5072e+03	+28.5

In the calculations, the decibel parameter (dB) is used as the output amplitude ratio that is defined as follows [56]:

$$(dB) = 10\log(\frac{p}{p_0}) \quad (73)$$

where P_0 and P represent a reference power and electrical power, respectively, since P is proportional to the reference voltage X, thus, we have [56]:

$$(dB) = 10\log(\frac{X}{X_0})^2 = 20\log(\frac{X}{X_0}) \quad (74)$$

where X_0 represents a reference voltage, the absorption of nanoparticles in the microcantilever sandwich is associated with various numerical values; therefore, the better parameter is more sensitive to the absorbed mass. This value affects not only the natural frequency but also the amplitude range from the piezo-magneto-electric layer. Hence, these three parameters can be used as measurement parameters for the microcantilever sandwich as a mass sensor.

Figures 2 to 15 illustrate the effect of various parameters based on numerical values of properties and layer geometry concerning the amount of added mass to the tip of the piezo-magneto-electric microcantilever on the natural frequency and amplitude range in the first three vibration modes. Figure 2 shows the effect of the input voltage on the piezo-magneto-electric layer for numerical values of 10, 20, and 30 *mV* in the first three vibration modes. As indicated by the presented results in Figure 2, for different input voltage values to the piezo-magneto-electric sensor layer, the Frequency Response Function (FRF) amplitude (dB) versus the excitation frequency is plotted. It is seen that when the natural frequency is close to the excitation frequency, the resonance phenomenon occurs. Consequently, the selection of various input voltage values for the microcantilever sandwich minimally impacts the FRF amplitude, while its effect on the frequency is ignored. On the other hand, the input voltage is applied as the external factor on the FRF amplitude.

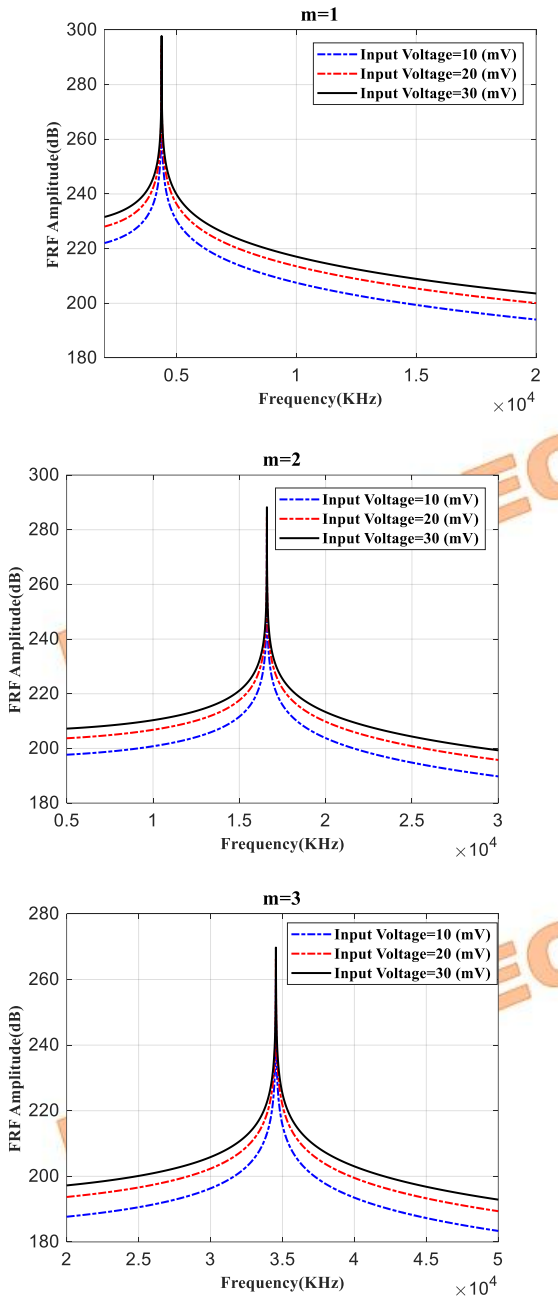

Fig 2. The effect of input voltage to the piezo-magneto-electric layer on the Frequency Response Function (FRF) amplitude of the sandwich microbeam for the first three oscillation modes.

Considering the excitation and vibration of the sensor layer and the performance of the second layer as the measurement layer in the microcantilever sandwich, the amount of added mass to the tip of the microcantilever can be observed in Figure 3. In this figure, the sensitivity of the excitation frequency and FRF amplitude is illustrated. It is evident from the graph that the maximum sensitivity of the amplitude occurs for an added mass of 0.05 micrograms. Based on the presented findings, it is observed that with the increase of an added mass, the natural frequency decreases, because the mass matrix of the sandwich microbeam increases. The added mass not only affects the natural frequency but also alters the FRF amplitude in the first vibration mode. Therefore, the natural frequency and FRF amplitude from the piezo-magneto-electric layer can be utilized as parameters in the microcantilever sandwich as a mass sensor. It is shown that by increasing the values of the added mass from 0.001 to 0.01 and 0.05 microgram, the first natural frequency decreases 65.1% and 84.25%, respectively.

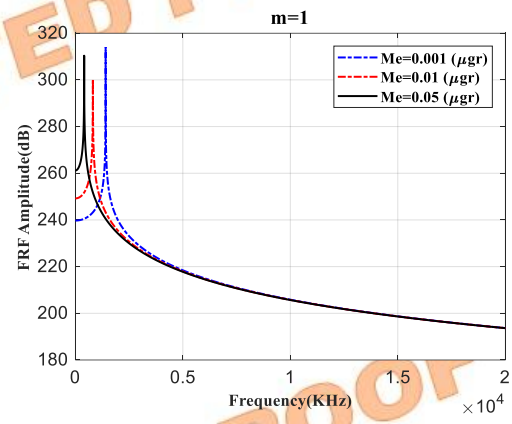

Fig 3. The effect of added mass on the FRF amplitude of a sandwich microbeam for the first oscillation mode.

In Figure 4, the effect of different densities for two cases, including case 1: copper, PZT-4, and gold, and case 2: titanium, Zn, and aluminum, on the natural frequency and FRF amplitude of a sandwich microbeam is presented. The density and Young's modulus of CNTRC for composite layers in the two cases are considered the same. It is evident from the figure that not only the natural frequency but also the FRF amplitude varies across the first two vibration modes for different material properties. It is shown that the natural frequency for case 1 is lower than that of case 2, because the Young's modulus to density ratio decreases. On the other hand, the ratio of stiffness to mass for case 1 is lower than that of case 2.

In Figure 5, the effect of different values of V_{CNT} and η_1 is related to the CNT layers on the FRF amplitude for the microcantilever in the first three vibration modes is shown. Considering the direct relationship between the volume fraction and the natural frequency, the increase in volume fraction has a noticeable effect on the frequency for higher modes. On the other hand, the increase in the volume fraction leads to enhanced stiffness of the sandwich microbeam, and then the natural frequency increases. It is shown that by increasing the values of the added mass from 12% to 17% and

28%, the first natural frequency enhances 3% and 9.3%, respectively.

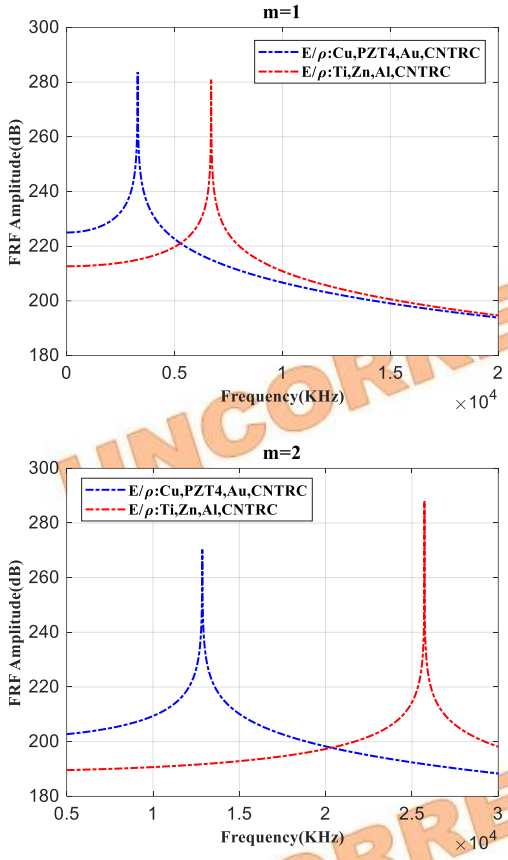

Fig 4. The effect of different Young's modulus and density on the FRF amplitude for a sandwich microbeam in the first two oscillation modes

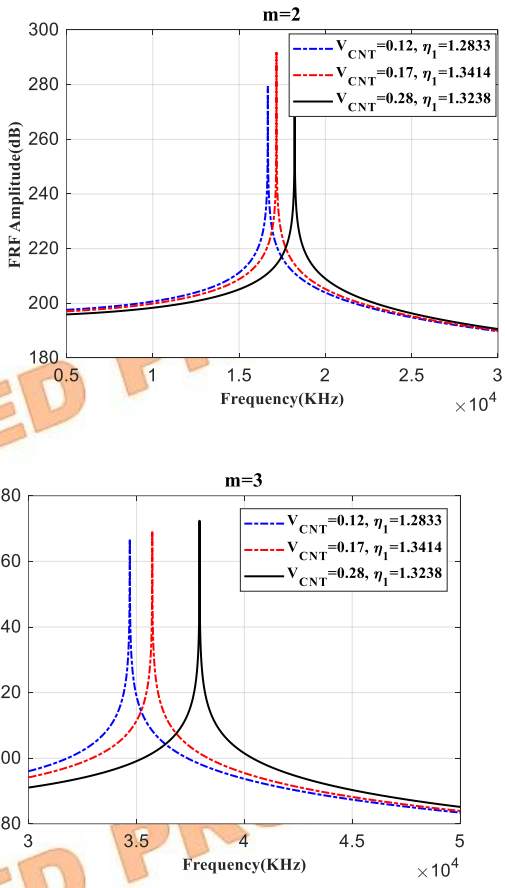

Fig 5. The effect of different values V_{CNT}, η_1, E_{11CNT}, and ρ_{CNT} related to the CNT layers on the FRF amplitude for the sandwich microbeam in the first three vibration modes.

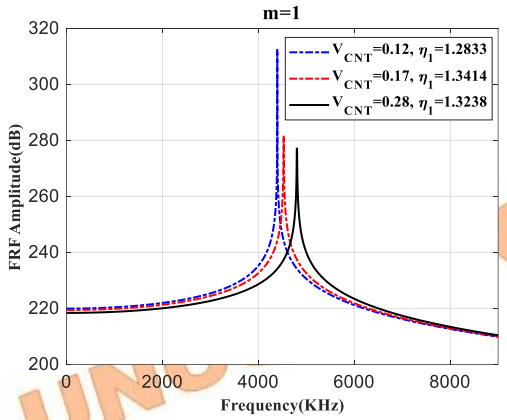

In Figure 6, the effect of different properties for the core as the main layer, including aluminum, gold, and titanium, on the FRF amplitude in the first three vibration modes is presented. According to the figure, with an increase in the stiffness-to-mass ratio, the natural frequency increases, because with an increase in this ratio, it is possible that the stiffness of the structure increases or the density decreases, which leads to an enhancement of the natural frequency. It is shown that the difference between curves for higher modes increases. It is shown that by decreasing E/ρ from Al to Ti and Au, the first natural frequency reduces from 15.21% and 36.18%, respectively.

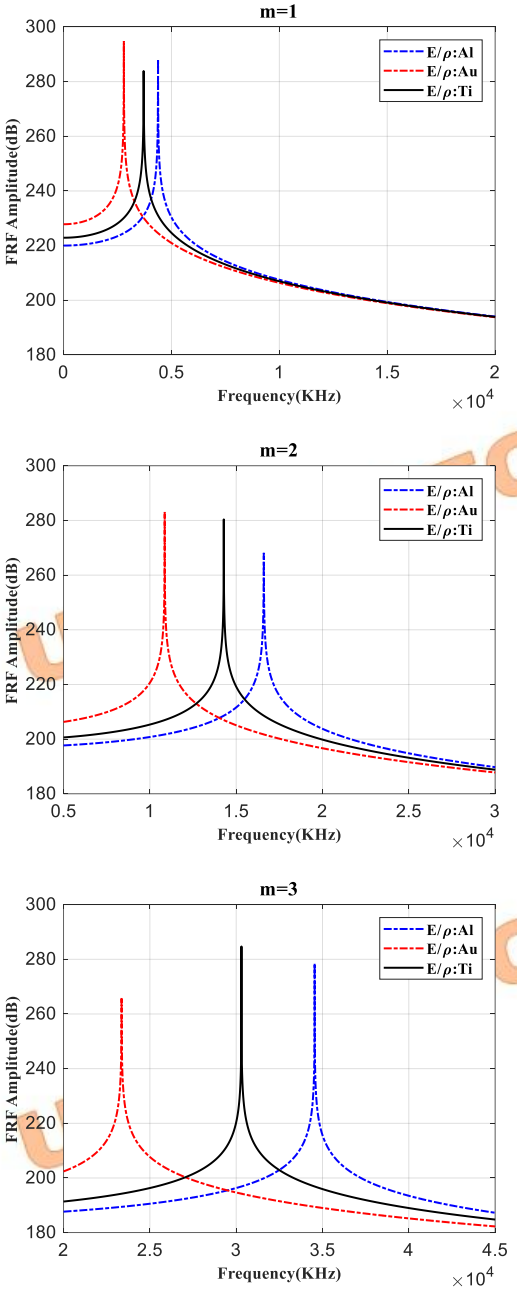

Fig 6. The effect of different properties for the core layer (aluminum, gold, and titanium) on the FRF amplitude of a sandwich microbeam in the first three oscillation modes.

In Figure 7, the significant effect of the length of the core layer to thickness ratio on the FRF amplitude for the microcantilever in the first vibration mode is shown. In these cases, as this ratio (L_1/H) increases, the stiffness of the sandwich microbeam decreases, thus leading to a reduction in the natural frequency of the microbeam. On the other hand, it becomes more flexible, resulting in a decrease in the natural frequency. It is shown that by increasing L_1/H from 10 to 15 and 20, the first natural frequency decreases from 55.08% and 74.64%, respectively.

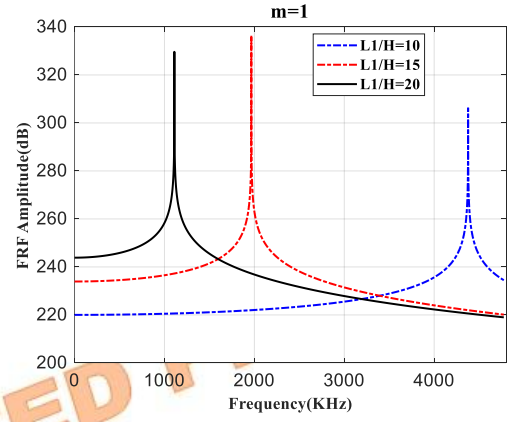

Fig 7. The effect of the aspect ratio of the core layer on the FRF amplitude for the sandwich microbeam in the first vibration mode.

In Figure 8, the effect of the length of eight layers on the length of core layer ratio on FRF amplitude for the sandwich microbeam is shown. It is illustrated that as the length of the eight layers is close to the length of the core, the natural frequency decreases, because the Young's modulus to density ratio decreases, and then the structure becomes more flexible. Thus, in this case, the natural frequency decreases. As this ratio increases, the stability of the sandwich microcantilever under the application of an external load (input voltage to the piezo-magneto-electric layer) reduces, and consequently, the natural frequency decreases. It is shown that by increasing L/L_1 from 0.6 to 0.8 and 1, the first natural frequency decreases from 43.28% and 63.56%, respectively.

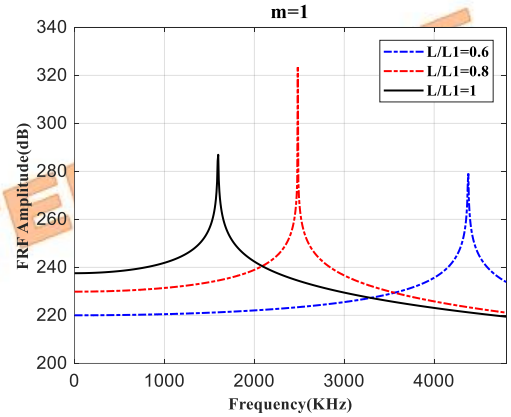

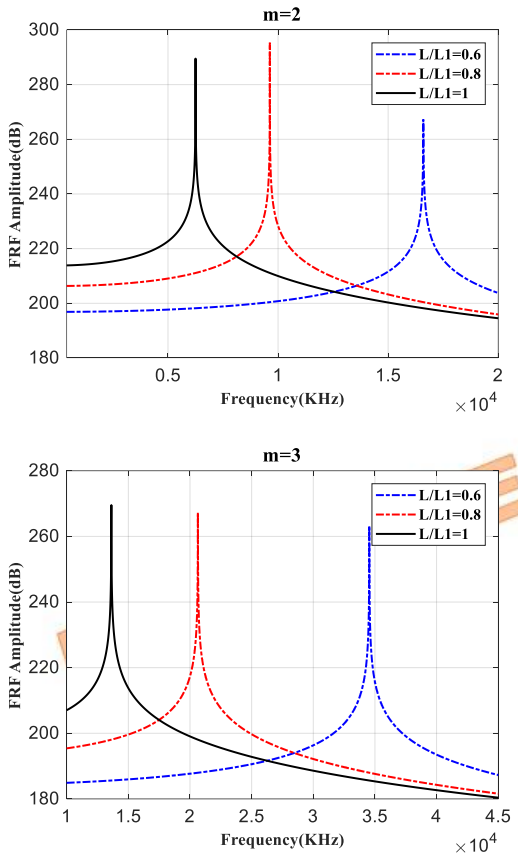

Fig 8. The effect of the length of eight layers on the length of core layer ratio on FRF amplitude for the sandwich microbeam.

The effect of various boundary conditions, including C-C, C-S, S-S, and C-F, on the natural frequency and amplitude of oscillations is also shown in Figure 9. It is considered that the natural frequency for C-C is higher than the other cases, because the stiffness of the structures increases.

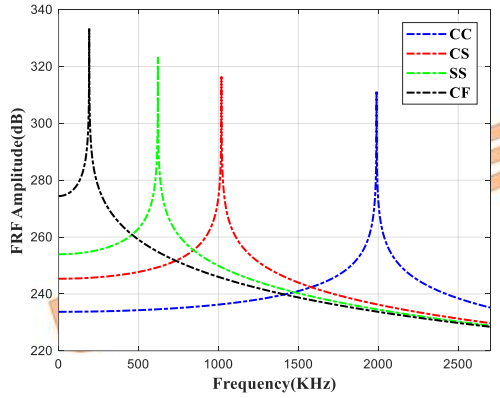

Fig 9. The effect of different boundary conditions based on ($L_1/H=10$, and h_c/h=0.8) on the FRF amplitude for the sandwich microbeam.

Figure 10 shows the dimensionless frequency for various boundary conditions of the sandwich microbeam in the first oscillation mode, which is compared with the other literature [55]. It is shown that there is a good agreement between them. On the other hand, the obtained results from various boundary conditions, including CC, CS, SS, and CF, have a good agreement with other references.

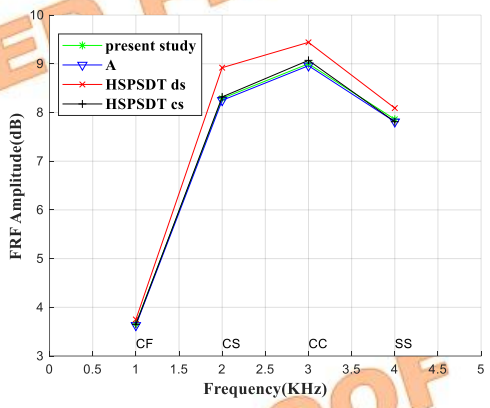

Fig 10. The validation of the present study is based on different boundary conditions with various theories in Ref. [55]. $\left(\bar{\omega} = (\omega L^2/h)\sqrt{\frac{\rho_f}{E_{2f}}}\right)$, L/H=5

Figure 11 shows the effect of the material length scale parameter on the FRF amplitude based on MCST at the micro scale in the first three vibration modes. It is shown that the natural frequency increases when considering the material length scale parameter. On the other hand, the natural frequency based on MCST ($l_m = 17.6\mu m$) is higher than classical theory (CT) ($l_m = 0$), because the material length scale parameter enhances the stiffness of a sandwich beam. On the other hand, the material length scale parameter leads to an increase in the stiffness of the sandwich microbeam, and then the natural frequency increases. It is shown that by considering the material length scale parameter, the first three natural frequencies increase 137.9%.

The purpose of presenting different distributions (CNTRC) in equations (8-12) is to analyze the dynamic behavior of the microbeam under various distributions of CNT. These distributions have been specifically used as reinforcement in a matrix to increase the stiffness of a sandwich beam. On the other hand, these effects are shown on the FRF amplitudes of the microbeam in Figure 12. The effects of these distributions, including functionally graded distributions (FG) FG-V, FG-O, FG-X, and uniform distribution (UD), on the dynamic behavior and

natural frequencies of the system are presented in Figure 12. It is shown from this figure that the natural frequency for FG-X is higher than the other distributions, because the stiffness of the structure at the furthest distance from the neutral axis; while the UD distribution becomes lower than the other cases, because the distribution of CNT in the thickness direction is the same.

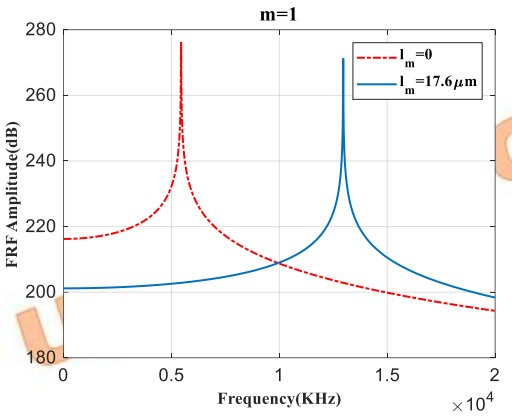

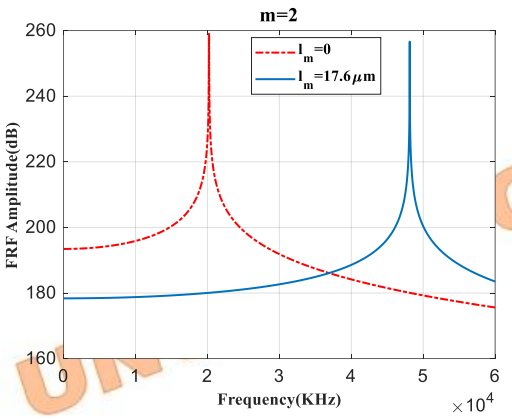

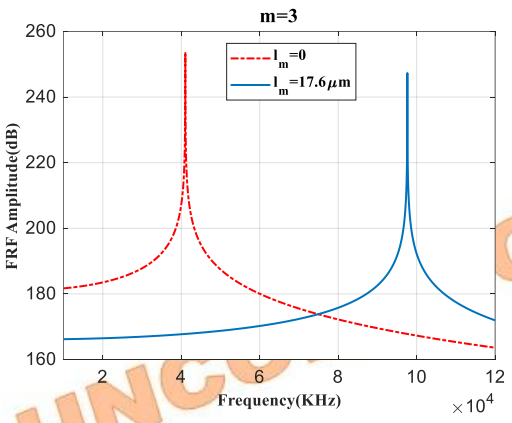

Fig 11. The effect of the material length scale parameter on the FRF amplitude based on MCST at the micro scale in the first three vibration modes.

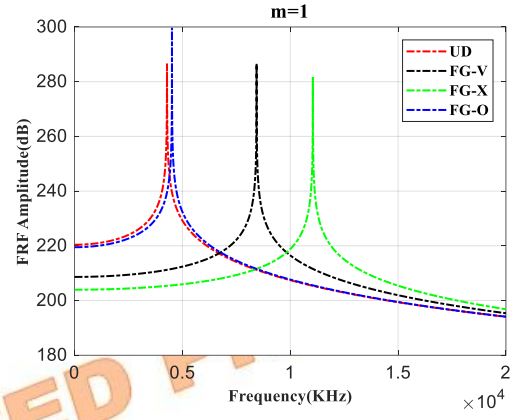

Fig 12. The effect of different CNTRC distributions on the FRF amplitude for the sandwich microbeam

Figure 13 shows the effect of different volume fractions on the frequency response for the micro sandwich beam. It is shown that with an increase in the volume fraction of the CNT, the stiffness of the structure enhances, and then it leads to an increase in the natural frequency.

The Young's modulus to density ratio for the nine-layer is shown as follows:

$$\frac{E}{\rho}\left(\frac{MPa}{kg/m^3}\right)=\begin{Bmatrix}4.09 & 11.08 & 4.09\\ 56.89 & 25.56 & 56.89\\ 4.09 & 11.08 & 4.09\end{Bmatrix}$$

Furthermore, considering the significant effect of geometric parameters on the sensitivity of the piezo-magneto-electric sandwich micro-cantilever beam as a mass sensor, the length and thickness parameters of the layers are also investigated. Additionally, the thickness ratio (the ratio of the core thickness to the total thickness) on the frequency response function (FRF) is also studied. Figure 14 shows the effect of the thickness ratio on the frequency response of the micro sandwich beam. It is shown that with an increase in the thickness ratio, the Young's modulus to density ratio for core is 25.56 that it is lower than nanocomposite layer (56.89), and the thickness ratio for the core is 0.6H, while the thickness ratio for the nanocomposite layer is 0.05H, thus the stiffness of core by increasing thickness ratio increases, and then the natural frequency enhances. It is shown that by enhancing h_c/H from 0.6 to 0.8 and 0.9, the first natural frequency increases 16.1% and 28.5%, respectively.

Figure 15 shows the effect of different piezo-electro-magnetic fields on the frequency

response of the micro sandwich beam. It is shown that considering simultaneously electric and magnetic fields is higher than the other cases, because the stiffness of the micro beam is enhanced.

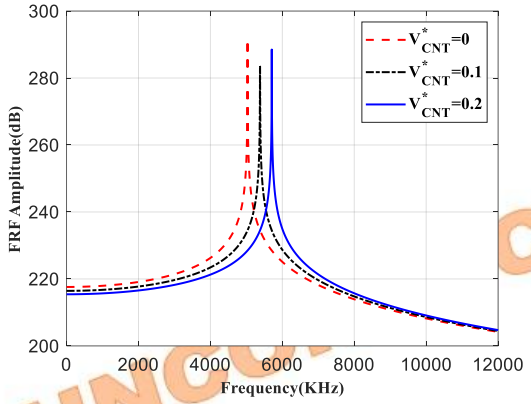

Fig 13. The effect of different volume fractions on the frequency response of the micro sandwich beam

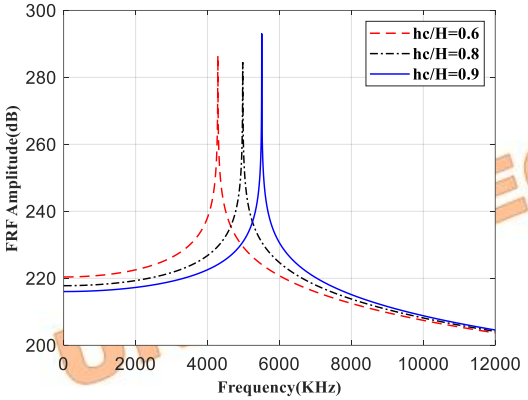

Fig 14. The effect of the thickness ratio on the frequency response of the micro sandwich beam

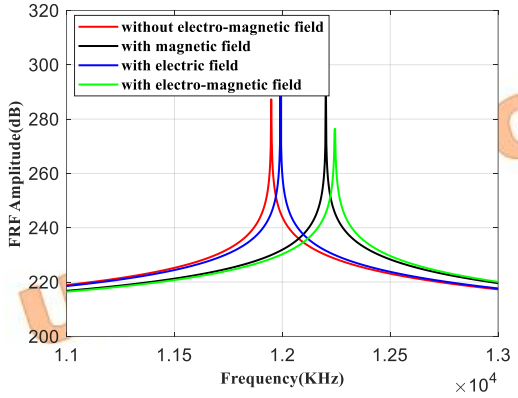

Fig 15. The effect of different piezo-electro-magnetic fields on the frequency response of the micro sandwich beam

Figure 16 shows the effect of the thickness of the electrode layer on the total thickness ratio ($h_{electrode}/H$) for hc/H=0.6 on the frequency response of the micro sandwich beam. It is shown that by increasing of $h_{electrode}/H$, the stiffness-to-weight ratio decreases, and then the natural frequency reduces.

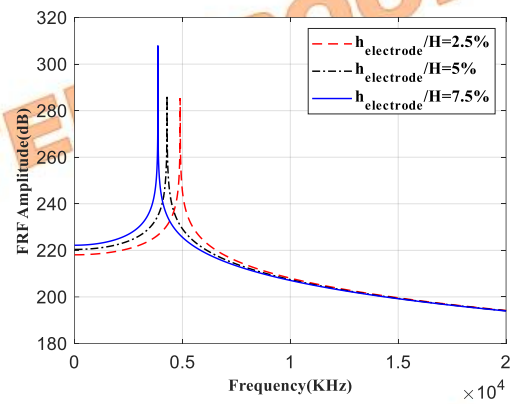

Fig 16. The effect of the thickness of the electrode layer on the total thickness ratio for hc/H=0.6 on the frequency response of the micro sandwich beam

6. Conclusion

In this study, the present work was to consider simultaneously forced vibration response of a nine-layer sandwich microbeam with homogeneous core reinforced by nanocomposite and piezo-magneto-electric layers as a self-sensing mass sensor at the end core layer based on two methods, including the separation of variables for different B.C.'s and Navier's method for the S-S case. These innovations in a nine-layer sandwich microbeam and methodological advancements clearly demonstrated the significant contribution of this study to the design of high-performance sandwich microbeams based on a self-sensing mass sensor. The convergence and accuracy of the present work were confirmed by comparing the obtained numerical results with those reported in the literature. Also, by employing Navier's solution method, the frequency response function(FRF) amplitude with and without considering the material length scale parameter based on the modified couple stress theory was considered. Moreover, based on the separation of variable method, the FRF amplitude for various boundary conditions, including C-C, S-S, C-S, and C-F, was illustrated. In this study, the influences of various parameters, such as an added mass at the end of core layer, different Young's modulus to the density ratio for two cases (case 1: copper, PZT-

4, and gold and case 2: titanium, Zn, and aluminum), different properties of core, volume fraction and various distributions of CNT, thickness ratio, aspect ratio, length of each layer to core layer ratio, material length scale parameter, electric and magnetic fields, and input voltage on the FRF amplitude were presented. The results were reviewed and analyzed with a focus on the key findings, design implications, and potential applications as follows:

1- The volume fraction of CNT has a direct relationship with the natural frequency of the microcantilever; as it increases, the effective stiffness of the beam increases, which leads to an enhancement of the natural frequency. Physically, increasing this parameter enhances the structure's bending resistance, resulting in a higher natural frequency. This finding indicated that by controlling this parameter, the FRF can be precisely tuned, optimizing the system's sensitivity for accurate volume fraction.

2- The geometric parameters, including the length of each layer to core layer (length ratio)(L/L_1), aspect ratio (L_1/H), the thickness of core to the total thickness ratio (thickness ratio) (h_C/H) on the FRF amplitude were presented. It is shown that with increasing length ratio and aspect ratio, the natural frequency reduces, because the structure becomes softer. Also, it is shown that with an increase in the thickness ratio, the natural frequency enhances. It is due to the Young's modulus to density ratio for the core being 25.56, which is lower than that of the nanocomposite layer (56.89) and higher than the other layer, but the thickness ratio for the core is 0.6H, while the thickness ratio for the nanocomposite layer is 0.05H; thus, the stiffness of the core by increasing thickness ratio increases. Physically, increasing the length ratio of the beam or aspect ratio reduces the beam's resistance to bending, allowing it to deform more easily. This finding has important design implications that, by precisely adjusting the dimensions and geometric ratios, the dynamic response and sensitivity of the system can be optimized.

3- Increasing the input voltage to the piezo-magneto-electric layer affects the FRF amplitude. The system's natural frequency primarily depends on the physical properties of the beam, such as its mass and stiffness, and changing the input voltage does not affect these parameters, so the natural frequency remains essentially constant. Physically, the input voltage only alters the energy supplied to the piezoelectric layer, which may slightly influence the FRF amplitude. This study indicated that to modify the natural frequency and optimize the system's dynamic response, designers should focus on selecting materials with appropriate mechanical properties and designing the structure's geometry, rather than adjusting the input voltage.

4- The effects of different boundary conditions, including C-C, C-S, S-S, and C-F, on the natural frequency and FRF amplitude were investigated. It is observed that the natural frequency is highest in the C-C condition. The physical explanation is that the C-C boundary condition clamps both ends of the beam; also, the deflection and slope of the beam at both ends are zero. Thus, the C-C boundary condition increases the effective stiffness of the structure and reduces its freedom of movement. With higher stiffness, the beam resists bending more effectively, which results in higher natural frequencies. This finding underscores the importance of selecting appropriate boundary conditions in the design of microsystems and sensors, as controlling constraints can optimize FRF and sensor sensitivity, ensuring precise and reliable performance of micro-magneto-electro-mechanical systems.

5- It is shown that the natural frequency based on MCST (l_m= 17.6 μm) is higher than that predicted by the classical theory (CT) (l_m= 0), because the material length-scale parameter increases the stiffness of the sandwich microbeam at the micro scale. Physically, the increase in this parameter accounts for small-scale effects of the material, which leads to a stiffer material than in comparison to the classical case. This finding highlights the importance of considering the small-scale effect in the precise design of microbeams.

6- Based on the obtained results, the highest sensitivity of the microbeam in the natural frequency response is observed by the value of the added mass at the end of the core layer. It is shown that the sensitivity of the excitation frequency and FRF amplitude is illustrated. It is considered that the maximum sensitivity of the amplitude occurs for an added mass of 0.05 micrograms. Based on the presented findings, it is observed that with the enhancement of an added mass, the natural frequency decreases, because the mass matrix of the sandwich microbeam increases. The added mass not only affects the natural frequency but also changes the FRF amplitude. Therefore, it can be considered as an important parameter to

control the natural frequency and FRF amplitude from the piezo-magneto-electric layer. This key finding enables designers to optimize sensor sensitivity by appropriately selecting the added mass, with applications in the design of microscale fluidic systems and microsensors.

7- Using different material properties (different Young's modulus to the density ratio for two cases (case 1: copper (Cu), PZT-4, and gold (Au) and case 2: titanium (Ti), Zn, and aluminum (Al)), different properties of core, such as aluminum, gold, and titanium) of the sandwich microbeam allows for a more accurate simulation of the real behavior of such structures. It is shown that the Young's modulus to density ratio for gold is lower than the other cases, because the stiffness to weight decreases, which leads to a reduction in natural frequency. Therefore, modeling the layers with their actual properties enables more precise prediction of dynamic response, natural frequencies, and sensor sensitivity. On the other hand, in many practical applications, sandwich microbeams are made of layers with different material properties to achieve desirable mechanical characteristics, such as a high strength-to-weight ratio. Considering and incorporating these varied properties in modeling provides a more accurate prediction of the behavior of such structures and can be applied in the design of lightweight systems in aerospace, robotics, and precision equipment. Also, it is highly valuable for designing lightweight and sensitive microbeams in precise sensors and micro-magneto-electro-mechanical applications.

8- It is shown that the natural frequency for the FG-X distribution is higher than for other distributions, because the stiffness of the structure at the furthest distance from the neutral axis. This behavior arises from the different distribution of mechanical properties along the beam: in FG-X, the stiffness varies in a way that increases the beam's resistance to bending and distributes the vibrational energy more uniformly along the beam, resulting in a higher natural frequency. In contrast, in the UD distribution, where the properties are uniform, the beam is relatively more flexible, which leads to a reduction in the natural frequency in comparison to the other case.

9- It is shown from the figure that the effect of four piezo-electro-magnetic cases (without electro-magnetic field, with electric field, with magnetic field, with electro-magnetic field) on the FRF amplitude of the micro sandwich beam. It is shown that considering simultaneously electric and magnetic fields is higher than the other cases, because the stiffness of the micro beam is enhanced. These findings highlight the importance of selecting appropriate numerical values and relevant parameters and their impact on the design and sensitivity of a sandwich microbeam as a pizo-electro-magnetic field. Such results can assist engineers in optimizing system sensitivity by accurately determining parameters, thereby enabling the successful design of high-precision and practical microstructured sensors. The sensitivity of the piezo-magneto-electric sandwich microbeam, considering various parameter values on the FRF amplitude and natural frequency, is investigated. This key finding indicates that the design and tuning of the layer parameters directly affect the dynamic response of the system and can be utilized for precise sensing applications as well as for optimizing vibrational response in industrial or laboratory environments.

10- It is illustrated that by enhancing the thickness of the electrode layer to the total thickness ratio, the stiffness-to-weight ratio decreases, and then the natural frequency reduces. Thus, by considering this ratio, one can obtain the best ratio to provide the resonance phenomenon.

11- The importance of selecting appropriate numerical values and relevant parameters and their influence on the design and sensitivity of a sandwich microbeam as a self-sensing mass sensor is highly significant. The outcome of the present study can be vital in the application of robotics, such as actuators and robot arms, as well as the medical industry.

Acknowledgement

The authors would like to thank the referees for their valuable comments, and also thanks a lot for increasing the quality of the present work. They thank the Iranian Nanotechnology Development Committee for their financial support and the University of Kashan for supporting this work by Grant No. 1311761/5.

Funding Statement:

This work was supported by the Iranian Nanotechnology Development Committee and the University of Kashan [Grant No. 1311761/5].

Conflicts of Interest:

The author declares that there is no conflict of interest regarding the publication of this article.

Nomenclature

Ae^{rx}, $e^{i\omega t}$	Displacement (bending)
B_i	Magnetic displacement
c_{mn}	Intrinsic damping
D_i	Electric displacement
dB	Output amplitude ratio
E	Young's modulus
E_i	Electric field
E_c	Core Young's modulus
$\boldsymbol{E_m}$	Matrix elastic modulus
E_{11CNT}	Longitudinal elastic modulus
H	Total thickness
H_i	Magnetic field
h	Thickness of all layers except the main layer
h_C	Thickness of the main layer
I	Moment of inertia
$I^{(0)}$, $I^{(2)}$	Mass moment of inertia
$[J]$	Jacobian matrix
$[K]$	Stiffness matrix
L	Length of the main layer (core)
L_1	Length of all layers except the main layer
L/H	Slenderness ratio
l_m	Material length scale parameter
M_x	Bending moment
$M_{xy}^{(0)}$	Effect of the small-scale parameter
M_e	Added mass at the microbeam tip
$[M]$	Mass matrix
m_{ij}	Couple stress
P	Electric power
$P(t)$	Input voltage
P_0	Reference power
q_n	Generalized coordinates
T	Energy density
U	Strain energy
V_m	Matrix volume
V_{CNT}^*	Relative volume
V_{CNT}	Carbon nanotube volume
W	Width
W_{CNT}	Relative weight
w_0	Transverse displacement
X	Electric voltage
X_0	Reference voltage
z_n	Neutral axis position
ρ	Density
ρ_c	Core density
ρ_m	Matrix density
ρ_{CNT}	Carbon nanotube density
$\bar{\omega}$	Dimensionless frequency

References

1. Zhang, Y., Li, Y. and Li, S. 2024. Free vibration of porous FG magneto-electro-elastic microbeams in the hygrothermal environment based on the differential transformation method. *Journal of Intelligent Material Systems and Structures*, *35(3)*, pp. 253–269.
2. Ghaderi, R. 2023. Sensitivity analysis of piezoelectric microcantilever excitability as resonator. *International Journal of Advanced Design and Manufacturing Technology*, *16(3)*, pp. 31–37.
3. Togun, N. and Bağdatli, S.M. 2024. Application of modified couple-stress theory to nonlinear vibration analysis of nanobeam with different boundary conditions. *Journal of Vibration Engineering & Technologies*, *12(4)*, pp. 6979–7008.
4. Arabzadeh-Ziari, M., Mohammadimehr, M., Arabzadeh-Ziari, E. and Asgari, M. 2024. Deflection, buckling and vibration analyses for a sandwich nanocomposite structure with foam core reinforced with GPLs and SMAs based on TSDBT. *Journal of Computational Applied Mechanics*, *55(2)*, pp. 289–321.
5. Liu, D., Su, J., Zhao, L. and Shen, X. 2024. State-space formulation for buckling and free vibration of axially functionally graded graphene reinforced nanocomposite microbeam under axially varying loads. *Materials*, *17(6)*, 1296.
6. Hosseini, S., Rahimi, G. and Anani, Y. 2021. A meshless collocation method based on radial basis functions for free and forced vibration analysis of functionally graded plates using FSDT. *Engineering Analysis with Boundary Elements*, *125*, pp. 168–177.
7. Hosseini, S. and Nazari, R. 2025. Free and forced vibration analysis of FG-porous beams on variable elastic foundations: a comprehensive study using higher-order beam theory and meshless collocation method. *Archive of Applied Mechanics*, *95(9)*, 225.
8. Hosseini, S. and Nazari, R. 2025. A comprehensive approach to free vibration and multi-objective optimization of sinusoidal sandwich structures utilizing artificial neural networks: Numerical and experimental

validation. *Mechanics Based Design of Structures and Machines*, pp. 1–31.
9. Mogehi, M.K., Mohammadimehr, M. and Duc, N.D. 2024. Vibration analysis of a sandwich Timoshenko beam reinforced by GOAM/CNT with various boundary conditions using VIM. *Materials Science and Engineering: B*, *304*, 117364.
10. Yapanmış, B.E. 2023. Nonlinear vibration and internal resonance analysis of microbeam with mass using the modified coupled stress theory. *Journal of Vibration Engineering & Technologies*, *11(5)*, pp. 2167–2180.
11. Bargozini, F., Mohammadimehr, M., Dawi, E.A. and Salavati-Niasari, M. 2024. Buckling of a sandwich beam with carbon nano rod reinforced composite and porous core under axially variable forces by considering general strain. *Results in Engineering*, *21*, 101945.
12. Yousefi, A.H., Kiani, F. and Abedi, E. 2023. Active control of sandwich microbeams vibration with FGM and viscoelastic/ER core. *International Journal of Advanced Design & Manufacturing Technology*, *16(3),* pp. 71-87.
13. Zhao, J.L., Chen, X., She, G.L., Jing, Y., Bai, R.Q., Yi, J., … and Luo, J. 2022. Vibration characteristics of functionally graded carbon nanotube-reinforced composite double-beams in thermal environments', *Steel and Composite Structures*, *43(6)*, pp. 797–808.
14. Azarniya, O. and Rahimi, G.H. 2024. Numerical and experimental analysis of free vibrations and static bending of a sandwich beam with a hyperelastic core. *Mechanics Based Design of Structures and Machines*, *52(2)*, pp. 706–728.
15. Rao, W.F., Wang, Y.W., Li, A.Q., Zhou, S.S. and Zheng, Z.M. 2024. An electromechanical stimulation regulating model with flexoelectric effect of piezoelectric laminated micro-beam for cell bionic culture. *Scientific Reports*, *14(1)*, 6130.
16. Cao, D.X., Xia, W., Guo, X.Y. and Lai, S.K. 2021. Modeling and experiment of vibro-impact vibration energy harvester based on a partial interlayer-separated piezoelectric beam. *Journal of Intelligent Material Systems and Structures*, *32(8)*, pp. 817–831.
17. Arani, A.G., Farazin, A., Mohammadimehr, M. and Lenjannejadian, S. 2021. Energy harvesting of sandwich beam with laminated composite core and piezoelectric face sheets under external fluid flow. *Smart Structures and Systems*, *27(4)*, pp. 641–650.
18. Alambeigi, K., Mohammadimehr, M. and Bamdad, M. 2023. An analytical study on free vibration of magneto electro micro sandwich beam with FG porous core on Vlasov foundation. *Advances in Nano Research*, *15(5)*, pp. 423-439.
19. Yu, P., Leng, W., Peng, L., Suo, Y. and Guo, J. 2021. The bending and vibration responses of functionally graded piezoelectric nanobeams with dynamic flexoelectric effect. *Results in Physics*, *28*, 104624.
20. Eghbali, M. and Hosseini, S.A. 2023. A complex solution on the dynamic response of sandwich graphene-reinforced aluminum-based composite beams with copper face sheets under two moving constant loads on an elastic foundation. *International Journal of Mechanical System Dynamics*, *3(3)*, pp. 251–264.
21. Duan, X., Cao, D., Li, X. and Shen, Y. 2021. Design and dynamic analysis of integrated architecture for vibration energy harvesting including piezoelectric frame and mechanical amplifier. *Applied Mathematics and Mechanics*, *42(6)*, pp. 755–770.
22. Asgari, M., Mohammadimehr, M., Arabzadeh-Ziari, M. and Arabzadeh-Ziari, E. 2025. Static bending, vibration, and buckling responses of a sandwich beam composed of five layers considering honeycomb core and CNTRC with SMA particles and temperature-dependent material properties using SSDT', *Mechanics of Advanced Composite Structures*, *12(1)*, pp. 153–168.
23. Arabloo Faraji, M.J., Ghorbanpour Arani, A., Mamnoun, E. and Khoddami Maraghi, Z. 2025. Vibration analysis of sandwich beams with magnetorheological elastomer core and FGM graphene nanoplatelet-reinforced polymer faces on viscoelastic foundation. *Mechanics of Advanced Composite Structures*, *12(3)*, pp. 447-464.
24. Sajadian, S.A., Mohammadimehr, M. and Irani Rahaghi, M. 2025. Vibration response of a sandwich higher-order micro beam based on shear and normal deformation theory on Kerr elastic foundation with thickness stretching effect. *Mechanics of Advanced Composite Structures*, *12(3)*, pp. 645–670.

25. Pham, S.D., Karamanli, A., Wattanasakulpong, N. and Vo, T.P. 2024. A Quasi-3D theory for bending, vibration and buckling analysis of FG-CNTRC and GPLRC curved beams. *Structures*, *63*, 106431.
26. Liu, X., Pagani, A., Carrera, E. and Liu, X. 2024. Free vibration analysis of composite beams and laminated reinforced panels by refined dynamic stiffness method and CUF-based component-wise theory. *Composite Structures*, *337*, 118058.
27. Mohammadimehr, M. 2024. The effect of a nonlocal stress-strain elasticity theory on the vibration analysis of Timoshenko sandwich beam theory. *Advances in Nano Research*, *17(3)*, pp. 275–284.
28. Ebrahimi-Tirtashi, A., Mohajerin, S., Zakerzadeh, M.R. and Nojoomian, M.A. 2021. Vibration control of a piezoelectric cantilever smart beam by adaptive control system. *Systems Science & Control Engineering*, *9(1)*, pp. 542–555.
29. Ren, Y. and Qing, H. 2022. Elastic buckling and free vibration of functionally graded piezoelectric nanobeams using nonlocal integral models. *International Journal of Structural Stability and Dynamics*, *22(5)*, 2250047.
30. Tran, T.T., Esen, I. and Nguyen, D.K. 2024. Dynamic behaviour of an inclined FG-CNTRC sandwich beam under a moving mass. *Vietnam Journal of Science and Technology*, *62(2)*, pp. 359–373.
31. Masoodi, A.R., Ghandehari, M.A., Tornabene, F. and Dimitri, R. 2024. Natural frequency response of FG-CNT coupled curved beams in thermal conditions. *Applied Sciences*, *14(2)*, 687.
32. Azarniya, O. and Rahimi, G.H. 2024. Numerical and experimental analysis of free vibrations and static bending of a sandwich beam with a hyperelastic core. *Mechanics Based Design of Structures and Machines*, *52(2)*, pp. 706–728.
33. Rezaei, H. and Noorabadi, M. 2021. Numerical analysis of the microstructural and geometrical effects on the flexural behavior of sandwich structures with skin/core delamination. *International Journal of Maritime Technology*, *16*, pp. 111–121.
34. Navagale, N.S. and Barjibhe, R.B. 2021. Modal analysis of composite material plate to enhance its use in engineering applications by using FEA', *International Research Journal of Modernization in Engineering Technology and Science*, *3(7)*, pp. 559–567.
35. Al-Bahrani, M. and Mahmoud, H.M. 2024. Indentation of sandwich beams: Comparison of Vlasov, Winkler, and shear theories with composite surfaces reinforced by CNTs and ANN model. *International Journal of Non-Linear Mechanics*, *160*, 104662.
36. Belabed, Z., Tounsi, A., Bousahla, A.A., Tounsi, A. and Yaylacı, M. 2024. Accurate free and forced vibration behavior prediction of functionally graded sandwich beams with variable cross-section: A finite element assessment. *Mechanics Based Design of Structures and Machines*, *52(11)*, pp. 9144-9177.
37. Fu, T., Hu, X. and Yang, C. 2023. Impact response analysis of stiffened sandwich functionally graded porous materials doubly-curved shell with re-entrant honeycomb auxetic core. *Applied Mathematical Modelling*, *124*, pp. 553–575.
38. Yu, Y., Fu, T., Wang, S. and Yang, C. 2025. Dynamic response of novel sandwich structures with 3D sinusoid-parallel-hybrid honeycomb auxetic cores: The cores based on negative Poisson's ratio of elastic jump. *European Journal of Mechanics-A/Solids*, *109*, 105449.
39. Rahimijonoush, A., Honarpisheh, M., Abdollahi, A. and Mohammadimehr, M. 2026. Experimental investigation of residual stress measurement on cold roll bonded Al/Cu composite by incremental hole-drilling method. *Mechanics of Advanced Composite Structures*, *13(1)*, pp. 1–11.
40. Tumkur Sadashivaiah, M.K., Joladarashi, S. and Kulkarni, S.M. 2025. Comparative study on impact responses of sandwich composites with stiff and compliant core materials. *Mechanics of Advanced Composite Structures*, *12(3)*, pp. 483–496.
41. Esen, İ., Koç, M.A. and Eroğlu, M. 2024. Effect of functionally graded carbon nanotube reinforcement on the dynamic response of composite beams subjected to a moving charge. *Journal of Vibration Engineering & Technologies*, *12(3)*, pp. 5203–5218.
42. Thinh, N.V. and Tung, H.V. 2024. Nonlinear dynamical characteristics of carbon nanotube-reinforced composite beams with piezoelectric actuators and elastically restrained ends under

thermo-electro-mechanical loads. *Journal of Thermoplastic Composite Materials*, *37(11),* pp. 3460-3491.
43. Amini, A., Mohammadimehr, M. and Faraji, A. 2019. Active control to reduce the vibration amplitude of the solar honeycomb sandwich panels with CNTRC facesheets using piezoelectric patch sensor and actuator. *Steel and Composite Structures*, *32(5)*, pp. 671–686.
44. Amini, A., Mohammadimehr, M. and Faraji, A. 2020. Optimal placement of piezoelectric actuator/sensor patches pair in sandwich plate by improved genetic algorithm. *Smart Structures and Systems*, *26(6)*, pp. 721–733.
45. Sakman, L.E., Ozer, H.O., Sezgin, A., Durak, B. and Kapkin, S. 2024. Eigenfrequencies of a three-dimensional arbitrarily-curved beam. *Journal of Vibration Engineering & Technologies*, *12*, pp. 7641–7651.
46. Shahraki, Z.N. and Ghaderi, R. 2019. Vibration and sensitivity analysis of piezoelectric microcantilever as a self-sensing sensor. *The European Physical Journal Applied Physics*, *87(2)*, 20401.
47. Ghaderi, R., Dehkordi, B.M. and Fard, A.R. 2021. Vibration and sensitivity analysis of double-layered non-uniform piezoelectric microcantilever as a self-sensing mass sensor. *Physica Scripta*, *96(11)*, 115205.
48. Ghaderi, R. 2023. Sensitivity analysis of piezoelectric microcantilever excitability as resonator. *International Journal of Advanced Design and Manufacturing Technology*, *16(3)*, pp. 31–37.
49. Khosravi, M. and Ghaderi, R. 2021. Vibration analysis and sensitivity analysis of semi-submerged multilayer piezoelectric microcantilever. *International Journal of Advanced Design & Manufacturing Technology*, *14(4)*, pp. 11-18.
50. Korayem, M.H. and Ghaderi, R. 2013. Vibration response of a piezoelectrically actuated microcantilever subjected to tip–sample interaction. *Scientia Iranica*, *20(1)*, pp. 195–206.
51. Amirabadi, H., Mottaghi, A., Sarafraz, M. and Afshari, H. 2024. Free vibrational behavior of a conical sandwich shell with a functionally graded auxetic honeycomb core. *Journal of Vibration and Control*, *31(7-8)*, pp.1223-1240.
52. Tran, T.T., Esen, I. and Nguyen, D.K. 2024. Dynamic behaviour of an inclined FG-CNTRC sandwich beam under a moving mass. *Vietnam Journal of Science and Technology*, *62(2)*, pp. 359–373.
53. Pham, S.D., Karamanli, A., Wattanasakulpong, N. and Vo, T.P. 2024. A Quasi-3D theory for bending, vibration and buckling analysis of FG-CNTRC and GPLRC curved beams', *Structures*, *63*, 106431.
54. Santos, J.A.D. and Reddy, J.N. 2012. Vibration of Timoshenko beams using non-classical elasticity theories. *Shock and Vibration*, *19(3)*, pp. 251–256.
55. Han, B., Hui, W.W., Zhang, Q.C., Zhao, Z.Y., Jin, F., Zhang, Q. and Lu, B.H. 2018. A refined quasi-3D zigzag beam theory for free vibration and stability analysis of multilayered composite beams subjected to thermomechanical loading', *Composite Structures*, *204*, pp. 620–633.
56. Imeci, S.T. and Temur, K. 2021. Center-slotted wideband hybrid 10 dB coupler. *Journal of Engineering Research Online First Article*, *11* (1), pp. 285-296.
57. Shahedi, S. and Mohammadimehr, M. 2020. Vibration analysis of rotating fully-bonded and delaminated sandwich beam with CNTRC face sheets and AL-foam flexible core in thermal and moisture environments. *Mechanics Based Design of Structures and Machines*, *48(5)*, pp. 584–614.
58. Bağdatli, S.M. and Togun, N. 2024. Nonlinear vibrations of a nanobeams rested on nonlinear elastic foundation under primary resonance excitation. *Iranian Journal of Science and Technology, Transactions of Mechanical Engineering*, *48(3)*, pp. 1243–1261.
59. Ansari, R., Ashrafi, M.A. and Hosseinzadeh, S. 2014. Vibration characteristics of piezoelectric microbeams based on the modified couple stress theory. *Shock and Vibration*, *2014(1)*, 598292.
60. Arai, M. and Masui, K. 2024. One-dimensional thermo-elastic wave analysis for dynamic thermoelasticity coupled with dual-phase-lag heat conduction model. *Mechanical Engineering Journal*, *11(5)*, 24-00255-24-00255.
61. Nguyen, B.H., Torri, G.B. and Rochus, V. 2024. Physics-informed neural networks with data-driven in modeling and characterizing piezoelectric micro-bender. *Journal of Micromechanics and Microengineering*, *34(11)*, 115004.
62. Nguyen, B.H., Czarnecki, P., Zunic, M., Torri, G.B. and Rochus, V. 2023.

Modeling of ferroelectric micro-cantilever actuator. in *2023 Symposium on Design, Test, Integration & Packaging of MEMS/MOEMS (DTIP)*, pp. 1–6. IEEE.

63. Nguyen, B.H., Nanthakumar, S.S., Zhuang, X., Wriggers, P., Jiang, X. and Rabczuk, T. 2018. Dynamic flexoelectric effect on piezoelectric nanostructures. *European Journal of Mechanics-A/Solids*, *71*, pp. 404–409.
64. Mohammadimehr, M., Firouzeh, S., Pahlavanzadeh, M., Heidari, Y. and Irani-Rahaghi, M. 2020. Free vibration of sandwich micro-beam with porous foam core, GPL layers and piezo-magneto-electric facesheets via NSGT. *Computers and Concrete: An International Journal*, *26(1)*, pp. 75–94.

Appendix A

The values of r_1, r_2, r_3, and r_4 are the roots of the differential equation for Eq. (58) (natural frequencies of the system) are obtained as follows:

$$bb = \sqrt{(e_{13}B^{(1)}y_5 + q_{13}B^{(1)}x_5 - I^{(2)}\omega^2)^2 - 4(-A^{(2)} - \frac{1}{2}B^{(0)})(I^{(0)}\omega^2)}$$

$$bc = (e_{13}B^{(1)}y_5 + q_{13}B^{(1)}x_5 - I^{(2)}\omega^2)$$

$$r_1 = +\sqrt{\frac{-bc + bb}{2(-A^{(2)} - \frac{1}{2}B^{(0)})}},\ r_2 = -\sqrt{\frac{-bb + bc}{2(-A^{(2)} - \frac{1}{2}B^{(0)})}}$$

$$r_3 = +\sqrt{\frac{-bb - bc}{2(-A^{(2)} - \frac{1}{2}B^{(0)})}},\ r_4 = -\sqrt{\frac{-bb - bc}{2(-A^{(2)} - \frac{1}{2}B^{(0)})}} \quad \text{(A-1)}$$

Appendix B

The Jacobian matrix (J) based on the aforementioned shape functions, eigen value equation, various boundary conditions, and related continuity is expressed as follows:

(SS)

$$\begin{bmatrix}
0 & 1 & 0 & 1 & 0 & 0 & 0 & 0 \\
0 & 0 & 0 & 0 & 0 & 1 & 0 & 1 \\
0 & EI\alpha_1^2 & 0 & -EI\alpha_2^2 & 0 & 0 & 0 & 0 \\
0 & 0 & 0 & 0 & 0 & EI\alpha_1^2 & 0 & EI\alpha_2^2 \\
\sinh\alpha_1 L_1 & \cosh\alpha_1 L_1 & \sin\alpha_2 L_1 & \cos\alpha_2 L_1 & -\sinh\alpha_1 L & \cosh\alpha_1 L_1 & \sin\alpha_2 L_1 & \cos\alpha_2 L_1 \\
\alpha_1\cosh\alpha_1 L_1 & \alpha_1\sinh\alpha_1 L_1 & \alpha_2\cos\alpha_2 L & -\alpha_2\sin\alpha_2 L_1 & -\alpha_1\cosh\alpha_1 L_1 & -\alpha_1\sinh\alpha_1 L_1 & -\alpha_2\cos\alpha_2 L & \alpha_2\sin\alpha_2 L_1 \\
0 & 0 & 0 & 0 & \sinh\alpha_1 L & \sinh\alpha_1 L & \sin\alpha_2 L & \cos\alpha_2 L \\
0 & 0 & 0 & 0 & EI\alpha_1^2\sinh\alpha_1 L + M_e\omega^2\sin(\frac{m\pi L_1}{L}) & EI\alpha_1^2\sinh\alpha_1 L + M_e\omega^2\sin(\frac{m\pi L_1}{L}) & -EI\alpha_2^2\sin\alpha_2 L + M_e\omega^2\sin(\frac{m\pi L_1}{L}) & -EI\alpha_2^2\cos\alpha_2 L + M_e\omega^2\sin(\frac{m\pi L_1}{L})
\end{bmatrix} \quad \text{(B-1)}$$

(CF)

$$\begin{bmatrix}
0 & 1 & 0 & 1 & 0 & 0 & 0 & 0 \\
0 & 0 & 0 & 0 & 0 & 1 & 0 & 1 \\
\alpha_1 & 0 & \alpha_2 & 0 & 0 & 0 & 0 & 0 \\
0 & 0 & 0 & 0 & \alpha_1 & 0 & \alpha_2 & 0 \\
\sinh\alpha_1 L_1 & \cosh\alpha_1 L_1 & \sin\alpha_2 L_1 & \cos\alpha_2 L_1 & -\sinh\alpha_1 L & \cosh\alpha_1 L_1 & \sin\alpha_2 L_1 & \cos\alpha_2 L_1 \\
\alpha_1\cosh\alpha_1 L_1 & \alpha_1\sinh\alpha_1 L_1 & \alpha_2\cos\alpha_2 L & -\alpha_2\sin\alpha_2 L_1 & -\alpha_1\cosh\alpha_1 L_1 & -\alpha_1\sinh\alpha_1 L_1 & -\alpha_2\cos\alpha_2 L & \alpha_2\sin\alpha_2 L_1 \\
0 & 0 & 0 & 0 & EI\alpha_1^3\sinh\alpha_1 L & EI\alpha_1^2\cosh\alpha_1 L & -EI\alpha_2^2\sin\alpha_2 L & -EI\alpha_2^2\cos\alpha_2 L \\
0 & 0 & 0 & 0 & EI\alpha_1^3\cosh\alpha_1 L + M_e\omega^2\sinh\alpha_1 L & EI\alpha_1^3\sinh\alpha_1 L + M_e\omega^2\cosh\alpha_1 L & -EI\alpha_2^3\cos\alpha_2 L + M_e\omega^2\sin\alpha_2 L & -EI\alpha_2^3\sin\alpha_2 L + M_e\omega^2\cos\alpha_2 L
\end{bmatrix} \quad \text{(B-2)}$$

(CC)

$$\begin{bmatrix}
0 & 1 & 0 & 1 & 0 & 0 & 0 & 0 \\
0 & 0 & 0 & 0 & 0 & 1 & 0 & 1 \\
\alpha_1 & 0 & \alpha_2 & 0 & 0 & 0 & 0 & 0 \\
0 & 0 & 0 & 0 & \alpha_1 & 0 & \alpha_2 & 0 \\
\sinh\alpha_1 L_1 & \cosh\alpha_1 L_1 & \sin\alpha_2 L_1 & \cos\alpha_2 L_1 & -\sinh\alpha_1 L & \cosh\alpha_1 L_1 & \sin\alpha_2 L_1 & \cos\alpha_2 L_1 \\
\alpha_1\cosh\alpha_1 L_1 & \alpha_1\sinh\alpha_1 L_1 & \alpha_2\cos\alpha_2 L & -\alpha_2\sin\alpha_2 L_1 & -\alpha_1\cosh\alpha_1 L_1 & -\alpha_1\sinh\alpha_1 L_1 & -\alpha_2\cos\alpha_2 L & \alpha_2\sin\alpha_2 L_1 \\
0 & 0 & 0 & 0 & \sinh\alpha_1 L & \cosh\alpha_1 L & \sin\alpha_2 L & \cos\alpha_2 L \\
0 & 0 & 0 & 0 & \alpha_1\cosh\alpha_1 L & \alpha_1\sinh\alpha_1 L & \alpha_2\cosh\alpha_2 L & -\alpha_2\cosh\alpha_2 L
\end{bmatrix} \quad \text{(B-3)}$$

(*CS*)

$$\begin{bmatrix} 0 & 1 & 0 & 1 & 0 & 0 & 0 & 0 \\ 0 & 0 & 0 & 0 & 0 & 1 & 0 & 1 \\ \alpha_1 & 0 & \alpha_2 & 0 & 0 & 0 & 0 & 0 \\ 0 & 0 & 0 & 0 & \alpha_1 & 0 & \alpha_2 & 0 \\ \sinh \alpha_1 L_1 & \cosh \alpha_1 L_1 & \sin \alpha_2 L_1 & \cos \alpha_2 L_1 & -\sinh \alpha_1 L & \cosh \alpha_1 L_1 & \sin \alpha_2 L_1 & \cos \alpha_2 L_1 \\ \alpha_1 \cosh \alpha_1 L_1 & \alpha_1 \sinh \alpha_1 L_1 & \alpha_2 \cos \alpha_2 L & -\alpha_2 \sin \alpha_2 L_1 & -\alpha_1 \cosh \alpha_1 L_1 & -\alpha_1 \sinh \alpha_1 L_1 & -\alpha_2 \cos \alpha_2 L & \alpha_2 \sin \alpha_2 L_1 \\ 0 & 0 & 0 & 0 & \sinh \alpha_1 L & \cosh \alpha_1 L & \sin \alpha_2 L & \cos \alpha_2 L \\ 0 & 0 & 0 & 0 & EI \alpha_1^2 \sinh \alpha_1 L & EI \alpha_1^2 \cosh \alpha_1 L & -EI \alpha_2^2 \sin \alpha_1 L & -EI \alpha_2^2 \cos \alpha_2 L \end{bmatrix} \quad \text{(B-4)}$$